Available online at www.sciencedirect.com
ScienceDirect
Lithos 94 (2007) 90–110
LITHOS
www.elsevier.com/locate/lithos

Modification of the subcontinental mantle beneath East Serbia: Evidence from orthopyroxene-rich xenoliths

Vladica Cvetković [a,b,*], Marina Lazarov [c], Hilary Downes [d], Dejan Prelević [a,e]

[a] Faculty of Mining and Geology, University of Belgrade, Đušina 7, 11000 Belgrade, Serbia and Montenegro
[b] Fachbereich für Geographie, Geologie und Mineralogie, Fakultät für Naturwissenschaften, Universität Salzburg, Hellbrunnerstraße 34/III, A-5020 Salzburg, Austria
[c] Institut für Mineralogie, Johann Wolfgang Goethe-Universität, Seckenberganlage 28, 60054 Frankfurt am Main, Germany
[d] Research School of Earth Sciences, Birkbeck College, Malet St., London, WC1E 7HX, UK
[e] Johannes Gutenberg-Universität, Institut für Geowissenschaften FB 22 Mineralogie, Becherweg 21, 55099 Mainz, Germany

Received 11 May 2005; accepted 23 December 2005
Available online 28 February 2006

Abstract

Orthopyroxene-rich olivine websterite xenoliths (OWB_2) in Palaeogene basanites in East Serbia are mostly composed of tabular low-Al_2O_3 orthopyroxene (>70 vol.%, Mg# 85–87) containing tiny Cr spinel inclusions. Orthopyroxene shows a slightly U-shaped primitive mantle-normalized trace element pattern with strong peaks at U and Pb, similar to that of orthopyroxene from normal regional peridotitic mantle. In between the orthopyroxenes are interstitial spaces composed of partially altered olivine (Mg# 85–87), clinopyroxene, Ti-rich spinel, Mg-bearing calcite, K-feldspar, apatite, ilmenite and relicts of a hydrous mineral. Clinopyroxene appears as selvages around orthopyroxene and as coarser euhedral crystals. Trace element patterns of the clinopyroxene selvages resemble those of adjacent orthopyroxene, whereas the coarser ones have flatter and more LREE- and LILE-enriched patterns, similar to that of metasomatic clinopyroxene. The OWB_2 xenoliths are interpreted as having formed in two stages. During Stage I orthopyroxene crystallized, along with some spinel, olivine and probably hydrous phase(s). This original OWB_2 lithology was a hydrous olivine-bearing orthopyroxenite that crystallised from subduction-related SiO_2-saturated, boninite-like magmas. During Stage II the interstitial minerals formed due to infiltration of a low-SiO_2, high-CaO and CO_2-rich external melt, accompanied by decomposition of original H_2O-bearing minerals. The calculated composition of the infiltrating liquid corresponds to a mafic alkaline melt similar to the basanitic host but more enriched in CO_2, LREE and LILE. Metasomatism is interpreted in terms of small degree melts related to the Palaeogene mafic alkaline magmatism.

Keywords: Geochemistry; Orthopyroxenite; Mantle; Xenoliths; East Serbia

1. Introduction

Most basalt-hosted mantle xenolith suites are dominated by anhydrous spinel lherzolites and harzburgites (Frey and Prinz, 1978; Menzies, 1983; Nicolas et al., 1987; Downes, 2001, and references therein). Pyroxene-rich xenoliths are less common and clinopyroxenites are generally more abundant than orthopyroxenites.

* Corresponding author. Fachbereich für Geographie, Geologie und Mineralogie, Fakultät für Naturwissenschaften, Universität Salzburg, Hellbrunnerstraße 34/III, A-5020 Salzburg, Austria. Fax: +43 662 8044 621.
E-mail address: vladica.cvetkovic@sbg.ac.at (V. Cvetković).

0024-4937/$ - see front matter © 2006 Elsevier B.V. All rights reserved.
doi:10.1016/j.lithos.2005.12.016

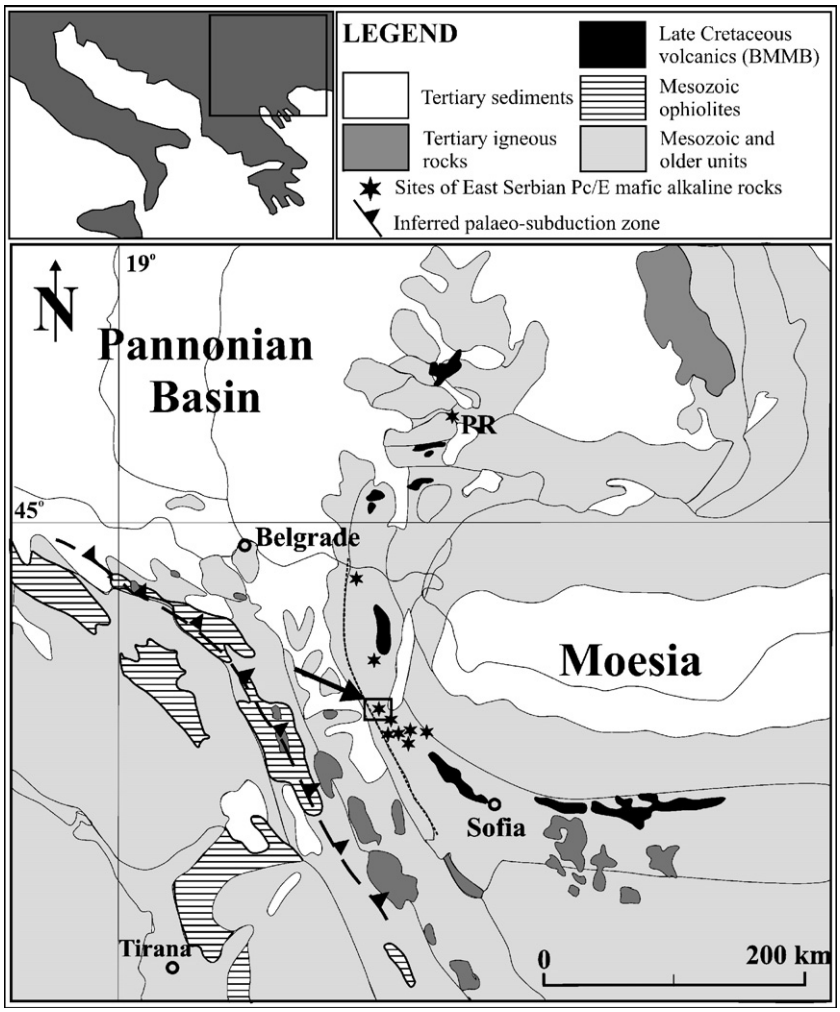

Fig. 1. Position of mantle xenolith-bearing East Serbian Palaeogene mafic alkaline rocks with respect to major geotectonic units; distribution of volcanic rocks of the subduction-related calc-alkaline belt (Berza et al., 1998), location of Poiana Rusca alkaline rocks (PR) and distribution of Palaeogene/Neogene Dinaride volcano-plutonic province are also shown; the arrow indicates the position of the studied orthopyroxene-rich xenoliths.

Orthopyroxene-rich rocks with subordinate olivine, clinopyroxene and hydrous phases have been described by McInnes and Cameron Eion (1994), Ertan and Leeman (1996), McInnes et al. (2001), Chane-Fo et al. (2003), Beccaluva et al. (2004), among others. Their origin has been variously interpreted but most occurrences are in sub-arc environments or supra-subduction zone ophiolites. Thus, the study of such orthopyroxene-rich material may help to elucidate palaeotectonic conditions of a lithospheric segment, especially the possible effects of subduction. Cvetković et al. (2004a) speculated that orthopyroxene-rich mantle xenoliths in Serbia also originated from arc-related magmas. Here we discuss major and trace element analyses of minerals in these xenoliths and demonstrate that they were originally orthopyroxenites containing some olivine and hydrous minerals, and that the latter have subsequently been decomposed by CO_2-rich fluid-induced melting. Precipitation of primary orthopyroxenite from high-Mg and high-Si magmas within the subcontinental mantle is an indication of melting of a highly refractory harzburgitic source due to a H_2O flux, commonly found in fore-arc regions. A tectonic setting involving eastward subduction under East Serbia is proposed for formation of these orthopyroxenites and their subsequent metasomatism.

2. Geological setting

Lithospheric xenoliths are found in Palaeogene basanites in East Serbia (Jovanović et al., 2001;

Cvetković et al., 2004b). These basanites occur along a north–south trending line within the Carpathian-Balkan unit of the Dinaride orogen (Fig. 1). Similar mantle xenolith-bearing rocks of Palaeogene age are found in Romania (Downes et al., 1995). This alkaline magmatism has important geodynamic implications, because it occurred along a line subparallel to a chain of Late Cretaceous calc-alkaline magmatic complexes (Cioflica et al., 1995; Vlad, 1997; Karamata et al., 1997; Berza et al., 1998; Ciobanu et al., 2002). Similar mafic alkaline volcanism slightly postdating subduction-related calc-alkaline magmatism worldwide (e.g. Hole and LeMasurier, 1994; Macera et al., 2003; Maughan et al., 2002) is mostly interpreted in terms of the slab-window model. If the Late Cretaceous calc-alkaline rocks were related to eastward subduction, then the East Serbian alkaline magmatism originated within a former fore-arc/arc region.

Cvetković et al. (2004a) proposed that the East Serbian mantle is predominantly composed of harzburgite and clinopyroxene-poor lherzolite, with subordinate dunite, all formed by depletion via extraction of basaltic

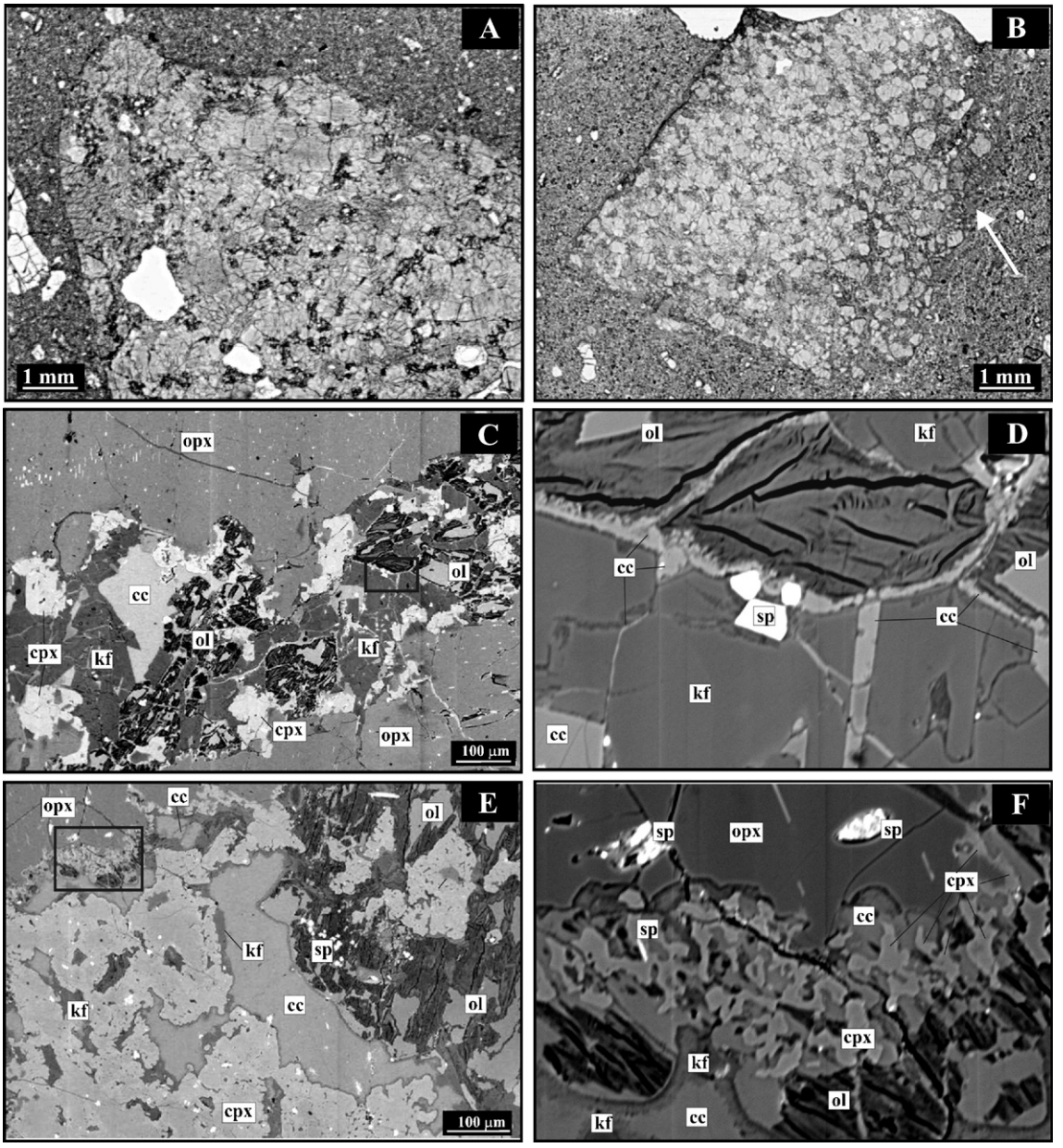

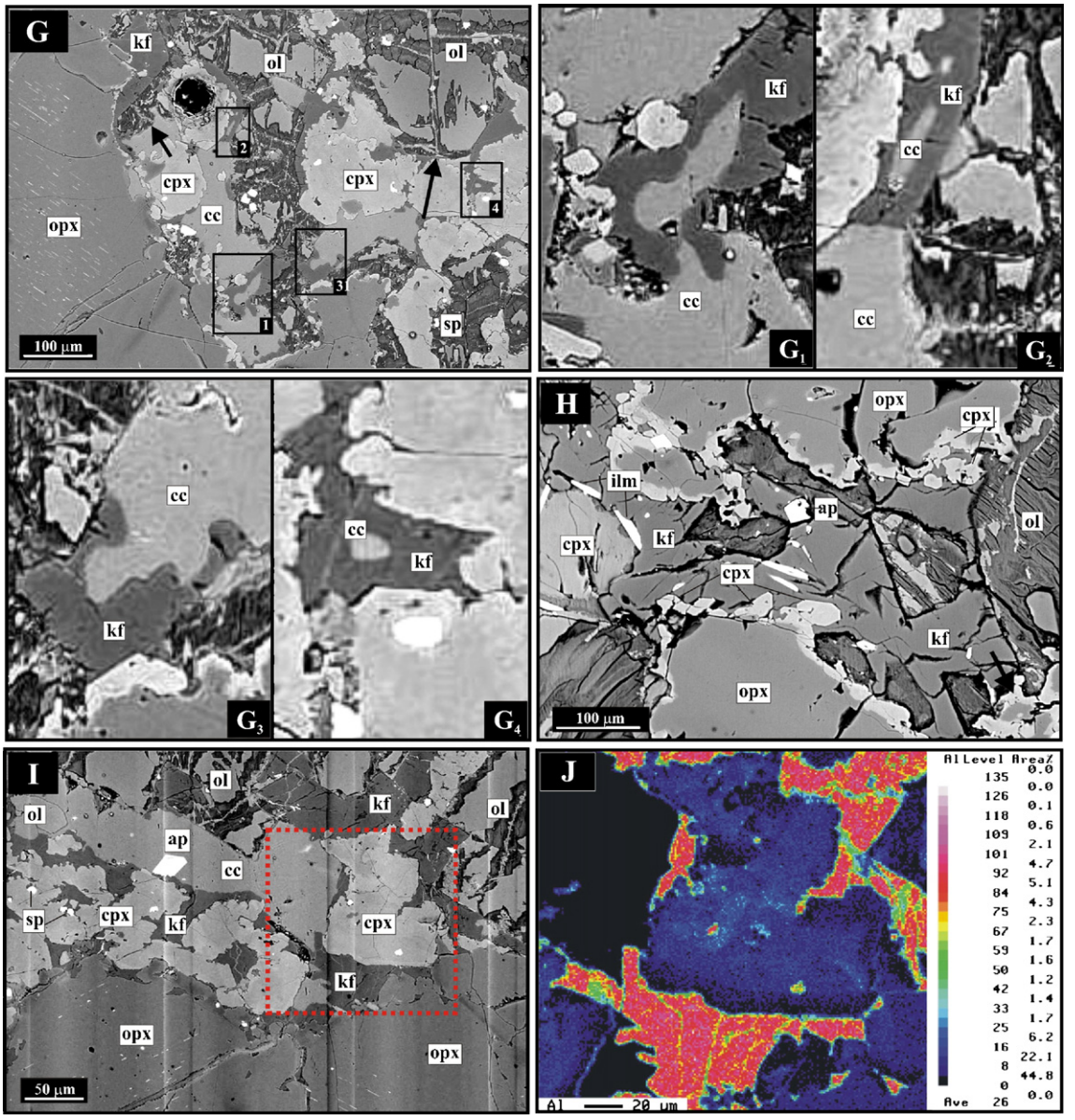

Fig. 2. Petrography and textural relationships of East Serbian orthopyroxene-rich xenoliths; (A, B) plane-polarized thin-section images of a coarse-grained (A) and fine-grained (B) xenolith; the coarse-grained xenolith has a sharp contacts with the basanitic host with a narrow reaction selvage; the margins of the fine-grained xenolith form a sharp angle, whereas the other side of the xenolith is partly disintegrated by the host material (arrow); both xenoliths show similar abundances of orthopyroxene crystals and interstitial patches, (C) a back-scatter electron (BSE) image of an interstitial assemblage rich in K-feldspar and poor in clinopyroxene; partially altered olivine crystals show skeletal growth; carbonate shows a negative crystal shape and forms sharp contacts with K-feldspar, (D) a detail from (C) (square), (E) a BSE image of an interstitial assemblage rich in clinopyroxene and poor in K-feldspar; clinopyroxene appears as selvages around orthopyroxene and as a network of euhedral/subhedral crystals, which sometimes enclose K-feldspar; carbonate displays a perfect negative crystal shape, often separated from the surrounding minerals by a narrow film of K-feldspar; (F) a detail from (E) (square) showing a reaction selvage around orthopyroxene; it is composed of olivine, clinopyroxene and glass; note that inclusion trails and exsolutions in orthopyroxene are cut by mineral phases in the selvage, (G) a BSE image of an irregular interstitial assemblage rich in clinopyroxene and poor in K-feldspar; very sharp contacts exist between olivine and K-feldspar in comparison to spongy rims of clinopyroxene-K-feldspar and olivine-carbonate interfaces (short arrow); fractures in olivine, which terminate at grain edges (long arrow); the black hole in the upper part of the image is a laser crater; (G1-G4) illustrate magnified details from (G) showing various relationships between K-feldspar and carbonate as well as carbonate blebs inside K-feldspar, (H) a BSE image of an interstitial assemblage with abundant needle-shaped ilmenite crystals; in the lower right corner (arrow) orthopyroxene relics enclosed by clinopyroxene selvage can be seen, (I) a BSE image of an irregular interstitial assemblage; note an idiomorphic olivine (upper left) and an apatite crystal enclosed by carbonate; dotted square shows the field of the X-ray maps presented in (J).

melts. We will use the abbreviations of Cvetković et al. (2004a) of D/HZ/L for these dunite/harzburgite/lherzolite xenoliths. They contain numerous pockets and veins filled by Cr-rich clinopyroxene, Ti-rich spinel, altered glass, apatite, ilmenite, phlogopite and rarely carbonate, formed from infiltration of alkaline melts. The same metasomatism also formed clinopyroxene-rich lherzolites, clinopyroxene (±olivine) megacrysts and spinel-rich olivine websterites (OWB_1). Cvetković et al. (2004a) also recognized spinel-poor orthopyroxene-rich xenoliths (OWB_2), which represent a subordinate lithology (less than 5% of the whole xenolith suite). A detailed petrographic description of these xenoliths is given below, with particular emphasis on textural relationships.

3. Petrography of OWB_2 xenoliths

The OWB_2 xenoliths are very dark in hand-specimen and rarely exceed 3 cm in diameter. They are undeformed with a granular structure (Fig. 2A,B). Four samples (M/SB2, M/SB6, X209 and X2011) are coarse-grained, with a grain size of 2–3 mm and two are fine-grained with grains <1 mm in diameter (X201 and X206). Both types have similar petrographic characteristics, although the fine-grained samples show more evidence of reaction with the host magma. Thus, fine-grained samples sometimes show partly disintegrated margins (Fig. 2B). The OWB_2 xenoliths are composed of two components: (a) the main crystal network of orthopyroxene and (b) minerals occurring within interstitial spaces. The latter include (in a general descending order of abundance) olivine, clinopyroxene, K-feldspar, carbonate, Cr-rich spinel, apatite and ilmenite. Modal proportions were estimated by analysis of scanned thin-section images (Table 1). Average modal proportions of mineral phases in the interstices were determined by image analysis of back-scattered electron (BSE) and transmitted-light photomicrographs. All these xenoliths are orthopyroxene-rich olivine websterites (Streckeisen, 1973).

Table 1
Results of modal analyses of East Serbian OWB_2 xenoliths

Sample no.	X201	X206	X209	X2011	M/SB2	M/SB6
Texture	FG	FG	CG	CG	CG	CG
Orthopyroxene	73.7	71.5	73.2	75.4	69.2	71.5
Olivine	8.3	10.5	11.5	8.7	11.3	10.4
Clinopyroxene	8.8	11.1	8.9	8.0	11.9	9.8
K-feldstar	6.4	4.1	3.5	3.9	4.7	5.6
Carbonate	0.9	2.1	1.8	2.8	2.0	1.9
Spinel	0.9	0.3	0.5	0.5	0.5	0.4
Apatite	0.6	0.2	0.3	0.4	0.3	0.3
Ilmenite	0.4	0.3	0.3	0.4	0.3	0.1

FG—fine-grained, CG—coarse-grained.

Orthopyroxenes form 70 to 76 vol.% and are unstrained tabular to slightly elongated crystals, sometimes closely packed, with triple junctions at nearly 120°. More often, they show strongly resorbed rims or are separated by wider and irregular interstitial spaces. They always contain narrow (≤1 μm) exsolution lamellae and euhedral/subhedral inclusions of Cr-spinel, usually a few μm in diameter. Along with the spinel inclusions, the orthopyroxene also contains numerous trails of tiny solid and/or fluid phases. Spinel exsolution lamellae and inclusion trails are often cut by the interstitial assemblages (Fig. 2F), suggesting that dissolution of orthopyroxene post-dated exsolution.

Olivine and clinopyroxene dominate the interstitial assemblages. They occur in roughly similar proportions and together occupy around 20% of the total rock volume. Olivine is always partially altered and often appears as skeletal crystals with euhedral terminations (Fig. 2C,E,G,H,I), forming sharp contacts to most other constituents (Fig. 2G). Alteration of OWB_2 olivine contrasts with olivines from D/HZ/L xenoliths, which are always fresh. It appears to be related to hydraulic fracturing and formation of phyllosilicates mostly along the cracks. The cracks terminate at olivine crystal surfaces, i.e. at interfaces between olivine and other minerals (Fig. 2G). Microprobe analyses of the alteration products revealed low totals of around 87 wt.%, with MgO ~22–26 wt.%, FeO ~10 wt.% and Al_2O_3 ~4 wt.%, probably corresponding to a non-stoichiometric mixture of phyllosilicates.

Clinopyroxene appears in two textural forms. Type 1 clinopyroxene forms irregular replacements/selvages around orthopyroxene (Fig. 2E,F,G,H). Sometimes, orthopyroxene relicts are enclosed within clinopyroxene grains (Fig. 2H, arrow). Type 2 clinopyroxene forms a network of subhedral to euhedral tabular crystals often with spongy rims when surrounded by K-feldspar (Fig. 2G,I). Sometimes tiny euhedral clinopyroxene grains of Type 2 are completely enclosed by carbonate, suggesting direct precipitation from a carbonate-rich melt/fluid.

K-feldspar has a variable modal abundance within the interstices, forming 3–6 vol.% of the total volume of the xenoliths. Very rarely, it is less abundant than carbonate and in a few patches it is more abundant than olivine. Glass of similar composition occurs instead of K-feldspar in some samples. Textural relationships show that K-feldspar crystallized after all other constituents and roughly simultaneously with the carbonate. K-feldspar and carbonate always enclose other minerals

and sometimes resorb them. Crystallization of these phases most probably occurred after alteration of olivine, as fractures related to olivine alteration do not propagate into K-feldspar and carbonate (Fig. 2G).

Carbonate shows sharp contacts with silicates and has a characteristic negative crystal shape (Fig. 2C,E,G, I), interpreted in terms of crystallization at depth instead of supergene precipitation. It is often surrounded by silicate glass rims, similar to those in xenoliths from Spitsbergen (Ionov et al., 1996) and Patagonia (Laurora et al., 2001). The co-existence of two liquids, one Si-, Al- and alkali-rich and the other of calciocarbonate composition, is evident from textural relationships that show irregular boundaries between K-feldspar and carbonate, as well as blebs of carbonate incompletely and/or completely surrounded by K-feldspar (Fig. 2G, see also magnified details). Co-existing feldspar and carbonate were also found in mantle xenoliths by Chalot-Pratt and Arnold (1999) and Delpech et al. (2004).

Spinel occurs as tiny isolated crystals or inclusion trails as well as narrow exsolutions in orthopyroxene, but is more abundant and coarser in the interstitial spaces. Here it is predominantly included in olivine and clinopyroxene, sometimes occurring as small accumulations of euhedral, prismatic to spongy grains (Fig. 2C,D, E,F,G) or attached to the surface of silicate crystals (Fig. 2D). Spinel is generally hosted by K-feldspar but never by carbonate. Apatite and ilmenite are generally rare and are absent in many interstitial patches. Apatite is euhedral (Fig. 2I) while ilmenite is often acicular (Fig. 2H). Apatite only occurs in carbonate whereas ilmenite is found only in K-feldspar/silicate glass. A few very small subhedral relicts of a pleochroic brownish mineral with the optical characteristics of phlogopite were also found in the interstices.

4. Mineral chemistry

Major element mineral analyses (Table 2) were performed using a wavelength-dispersive (WDS) electron microprobe at the University of Frankfurt and an energy-dispersive (EDS) electron microprobe at Birkbeck. The WDS machine was equipped with a five-spectrometer JEOL JXA 8900RL electron probe microanalyser. Analyses were performed using an acceleration potential of 15 kV, a beam current of 20 nA and a spot size of 3 μm, except for the small spinels where a defocused spot size of 1 μm was used. Data were reduced using the ZAF procedure. Analytical conditions for the Birkbeck EDS microprobe are given by Cvetković et al. (2004a). Analyses from both laboratories are in good agreement except for MnO contents in Cr-spinel, which are almost an order of magnitude lower in the WDS analyses, probably due to an overlap between Mn and Cr peaks in the EDS analyses. However, both EDS and WDS data revealed similar Cr# values.

Orthopyroxene has a uniform major element composition within individual samples. However, Mg# [MgO*100/(MgO+FeO)] in orthopyroxene from coarse-grained samples is 86–87 and in those from fine-grained samples ranges 84.5–85. They all have low Al_2O_3 (1.5–2.5 wt.%), Cr_2O_3 (mostly <0.4 wt.%) and CaO (<0.3 wt.%) contents. Fig. 3 shows that compared to orthopyroxene from East Serbian D/HZ/L xenoliths (Cvetković et al., 2004a), OWB_2 orthopyroxene displays similar Al_2O_3 and lower Mg#s and Cr_2O_3 and CaO concentrations. Low-Al orthopyroxenes in orthopyroxenite samples from Colorado (Smith et al., 1999) and Papua New Guinea (McInnes et al., 2001) show much higher Mg#s but orthopyroxene in xenoliths from W USA and SE Spain (Ertan and Leeman, 1996; Beccaluva et al., 2004) are similar to orthopyroxene from OWB_2 samples.

Olivines from the fine-grained OWB_2 xenoliths have lower forsterite contents (Fo_{82}–Fo_{86}) than those in the coarse-grained ones (Fo_{85}–Fo_{88}), but the overall ranges overlap. They tend to show slightly higher Mg#s than the co-existing orthopyroxene in contrast to the D/HZ/L xenoliths from Serbia (Cvetković et al., 2004a) and the Pannonian Basin (e.g. Embey-Isztin et al., 2001). OWB_2 olivines are distinctively less magnesian than those in the D/HZ/L (Mg#>90) but clearly more magnesian than those from the basanitic host (Mg#<75). CaO contents (~0.2 wt.%) are higher than in olivine from D/HZ/L xenoliths and comparable to those in olivine associated with clinopyroxene megacrysts (Cvetković et al., 2004a).

Clinopyroxene exhibits variable compositions throughout the whole suite and within individual samples, but there is no particular difference between the coarse-grained and fine-grained samples. It shows a wider range of Mg# (84–93) than do co-existing orthopyroxene and olivine. Al_2O_3 contents are also variable (0.34–4.43 wt.%), whereas Cr_2O_3 and TiO_2 contents are more uniform. Fig. 2J presents an X-ray map of Al distribution in a coarse clinopyroxene enclosed by K-feldspar and carbonate, showing Al-depletion of clinopyroxene rims in contact with K-feldspar. This implies that precipitation of K-feldspar occurred after crystallization of clinopyroxene, in agreement with other textural observations. Fig. 4 shows that Type 1 clinopyroxenes (formed at the expense of tabular

Table 2
Representative microprobe analyses of minerals from East Serbian OWB2 xenoliths

	Olivine					M/SB2					Orthopyroxene						
	M/SB2			M/SB6	X201						M/SB6			X201	X206	X209	X2011
SiO_2	40.07	39.59	39.93	39.72	39.86	55.52	55.77	55.85	55.11	55.54	55.47	55.46	55.46	55.50	55.86	56.51	55.51
TiO_2	0.02	0.02	0.00	0.02		0.06	0.07	0.03	0.05	0.06	0.07	0.06	0.06	0.09	0.13	0.14	0.05
Al_2O_3	0.03	0.01	0.03	0.03		2.07	1.87	1.69	1.90	1.75	2.02	1.88	1.99	1.99	1.90	1.91	1.72
FeO	10.38	11.77	11.80	13.38	13.90	8.83	8.87	8.85	8.86	8.79	8.89	8.86	8.86	9.83	10.24	8.83	8.95
MnO	0.18	0.20	0.21	0.23	0.25	0.19	0.18	0.20	0.19	0.19	0.17	0.19	0.19	0.18	0.15	0.04	0.13
MgO	49.21	48.23	48.00	46.77	44.80	32.75	32.86	33.33	32.68	32.94	32.64	32.84	32.79	31.47	31.39	32.68	32.21
CaO	0.19	0.18	0.22	0.19	0.14	0.17	0.17	0.18	0.19	0.18	0.18	0.18	0.18	0.21	0.19	0.22	0.19
Na_2O	0.02	0.02	0.01	0.02		0.02	0.01	0.02	0.03	0.00	0.05	0.02	0.02	0.48	0.33	0.40	0.44
K_2O	0.00	0.00	0.01	0.01		0.01	0.00	0.01	0.01	0.00	0.01	0.01	0.00				
Cr_2O_3	0.06	0.03	0.06	0.06		0.35	0.32	0.19	0.36	0.31	0.35	0.30	0.34	0.35	0.36	0.39	0.28
NiO	0.37	0.25	0.37	0.20	0.51	0.12	0.09	0.11	0.08	0.06	0.09	0.10	0.10				
P_2O5	0.02	0.00	0.03	0.03		0.00	0.01	0.00	0.00	0.00	0.00	0.00					
Total	100.54	100.31	100.67	100.65	99.45	100.10	100.22	100.45	99.47	99.83	99.92	99.92	99.99	100.09	100.55	101.14	99.48
Mg#	89.4	88.0	87.9	86.2	85.2	86.6	86.6	86.8	86.6	86.7	86.5	86.6	86.6	84.9	84.4	86.8	86.4

	Clinopyroxene-coarse									Clinopyroxene-opx-replacements							
	M/SB2		M/SB6		X201	X206	X209		X2011	M/SB2	M/SB6				X201	X2011	
SiO_2	53.17	52.54	52.22	51.90	51.66	53.08	52.28	52.28	53.52	51.96	53.44	52.00	52.34	53.08	52.01	52.46	52.43
TiO_2	0.22	0.31	0.61	0.41	0.38	0.37	0.42	0.42	0.72	0.34	0.36	0.58	0.40	0.46	1.07	0.41	0.39
Al_2O_3	2.28	2.89	3.21	3.75	4.43	2.49	2.93	2.93	0.94	3.15	1.28	2.72	3.29	1.82	0.89	2.61	2.64
FeO	2.84	3.40	2.60	2.97	3.24	3.52	4.13	4.13	3.93	4.22	4.46	3.88	5.41	4.79	4.65	4.93	5.25
MnO	0.10	0.10	0.08	0.06	0.12	0.17	0.13	0.13	0.33	0.12	0.19	0.15	0.14	0.19	0.98	0.26	0.40
MgO	19.50	18.46	18.86	18.71	17.74	18.23	17.97	17.97	17.31	18.07	18.39	16.55	18.00	18.59	17.98	17.73	17.17
CaO	19.43	19.69	19.88	19.53	20.55	20.74	19.40	19.40	21.51	18.00	18.65	21.11	18.05	18.31	17.45	18.91	18.66
Na_2O	0.49	0.58	0.47	0.52	0.43	0.55	0.55	0.55	0.66	0.64	0.89	0.73	0.86	0.76	1.73	0.69	0.80
K_2O	0.01	0.00	0.01	0.01			0.01	0.01		0.03	0.01	0.01	0.01	0.01			
Cr_2O_3	1.45	1.43	1.16	1.44	0.90	1.01	1.13	1.13	1.16	1.29	1.30	1.50	0.79	1.17	3.00	1.04	2.19
NiO	0.08	0.09	0.15	0.16			0.04	0.04		0.03	0.05	0.00	0.11	0.04			
P_2O5	0.01	0.02	0.00	0.00			0.01	0.01		0.01	0.00	0.02	0.00	0.01			
Total	99.58	99.50	99.26	99.46	99.46	100.15	99.01	99.01	100.09	97.87	99.03	99.24	99.41	99.22	99.76	99.04	99.93
Mg#	92.2	90.4	92.6	91.7	90.4	89.8	88.3	88.3	87.8	88.2	87.6	88.0	85.2	86.9	85.0	85.9	84.4

	Spinel from interstices									Spinel inside orthopyroxene							
	M/SB2		M/SB6		X209			X2011		M/SB2	M/SB6		X209	X 2011			
SiO_2	1.63	0.39	0.09	0.22	0.26	0.47	0.12	0.39	0.83	0.13	0.13	0.33	0.05	0.07	0.11	0.06	0.10
TiO_2	3.09	5.99	11.52	7.22	8.65	4.33	7.85	4.46	8.10	0.86	0.32	0.95	0.45	0.35	1.18	0.37	0.41
Al_2O_3	2.69	3.87	1.98	7.67	4.25	4.56	8.24	3.06	2.37	7.46	15.01	15.45	17.01	16.51	11.86	16.55	16.44
Cr_2O_3	47.88	40.86	36.78	39.79	34.76	45.69	33.73	46.49	40.58	50.73	44.14	43.63	48.25	45.39	47.78	44.90	45.66
FeOt	33.85	36.66	35.32	31.04	41.69	34.55	37.22	34.87	39.71	32.02	26.86	27.25	21.97	26.37	26.31	26.25	25.30
MnO	0.53	0.49	0.43	0.41	3.30	3.79	0.57	4.01	3.54	0.56	0.29	3.78	0.31	0.30	0.29	0.28	0.31
MgO	5.79	7.61	10.60	10.38	6.28	6.93	8.71	5.65	5.69	5.73	11.19	7.68	12.68	10.10	11.27	9.88	10.13
CaO	0.42	0.04	0.18	0.33	0.32	0.23	0.21	0.69	0.10	0.30	0.01	0.40	0.01	0.01	0.05	0.00	0.01
Total	95.87	95.91	96.91	97.05	99.52	100.56	96.64	99.62	100.92	97.79	97.94	99.48	100.73	99.09	98.85	98.29	98.36
Mg#	0.335	0.394	0.466	0.495	0.336	0.405	0.424	0.342	0.301	0.322	0.589	0.452	0.621	0.522	0.580	0.510	0.522
Cr#	0.923	0.889	0.933	0.783	0.850	0.872	0.732	0.912	0.923	0.821	0.662	0.651	0.660	0.645	0.732	0.645	0.645
Ti/Al	0.73	0.99	3.71	0.60	1.30	0.61	0.61	0.93	2.18	0.07	0.01	0.04	0.02	0.01	0.06	0.01	0.02

	Potash-feldspar							Unknown		Carbonate			Olivine alteration			Ilmenite	
	M/SB2		M/SB6		X201	X2011		X201		M/SB2	M/SB6		M/SB2	M/SB6		X209	X2011
SiO_2	65.22	65.44	66.46	65.48	62.90	63.90	SiO_2	52.13	SiO_2	0.01	0.03	SiO_2	48.69	46.83	46.38	0.45	0.28
TiO_2	0.48	0.47	0.27	0.40	0.12		TiO_2	5.54	TiO_2	0.00	0.00	TiO_2	0.07	0.03	0.00	52.87	51.31
Al_2O_3	19.92	18.83	19.19	18.65	19.35	18.52	Al_2O_3	1.23	Al_2O_3	0.00	0.01	Al_2O_3	4.01	3.62	3.18	0.17	0.05
FeO	0.32	0.54	0.59	0.62			FeO	4.10	FeO	0.13	0.38	FeO	8.79	10.44	10.16	33.80	34.02
MnO	0.00	0.02	0.02	0.03			MnO	0.04	MnO	0.11	0.47	MnO	0.03	0.05	0.03	0.44	0.45
MgO	0.01	0.04	0.06	0.14			MgO	17.99	MgO	2.61	2.34	MgO	22.62	24.98	25.98	7.95	7.61
CaO	0.24	0.05	0.02	0.05	0.00	0.05	CaO	5.67	CaO	58.31	55.82	CaO	0.96	0.93	0.94	0.12	1.15
Na_2O	5.60	4.79	6.18	5.91	2.99	3.27	Na_2O	3.67	Na_2O	0.00	0.01	Na_2O	0.05	0.08	0.03		
K_2O	8.71	9.69	8.04	8.36	8.72	8.60	K_2O	1.21	K_2O	0.05	0.00	K_2O	0.17	0.16	0.13		
Cr_2O_3	0.01	0.00	0.00	0.00			Cr_2O_3	0.85	Cr_2O_3	0.00	0.01	Cr_2O_3	0.05	0.09	0.06	2.16	2.21
NiO	0.01	0.00	0.04	0.00			NiO		NiO	0.00	0.00	NiO	0.22	0.20	0.30		
P2O5	0.04	0.04	0.09	0.06			P2O5		P2O5	0.01	0.08	P2O5	0.02	0.00	0.00		
Total	100.57	99.90	100.96	99.70	94.09	94.35	Total	92.41	Total	61.23	59.15	Total	85.68	87.41	87.18	97.96	97.07
							Mg#	0.891	Mg#	0.972	0.921	Mg#	0.823	0.813	0.824		
									Xca	0.94	0.93						

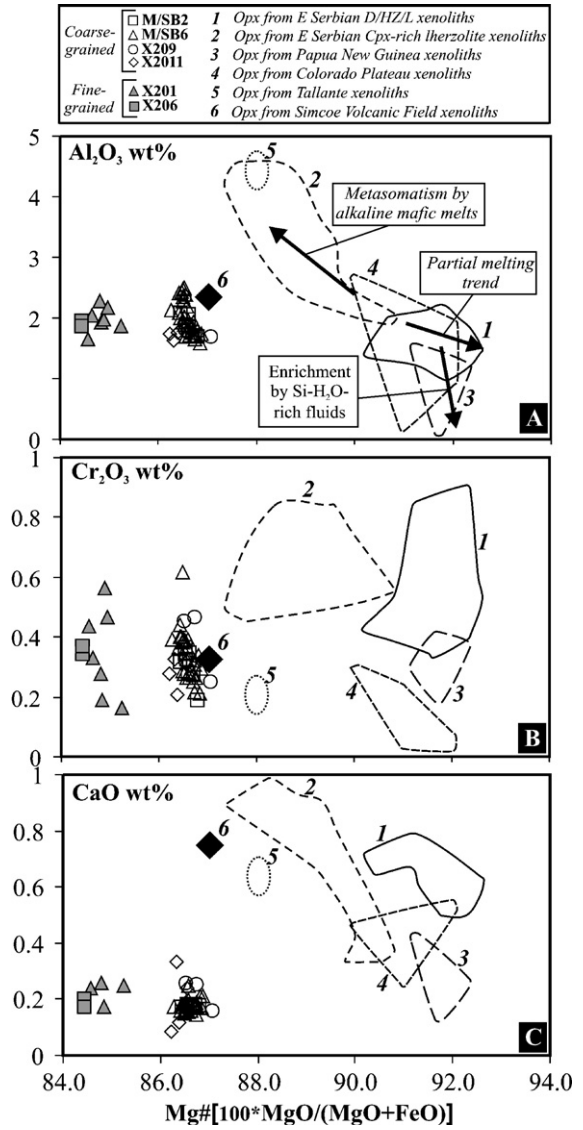

Fig. 3. Plots of Mg# [100*MgO/(MgO+FeO)] vs. Al_2O_3 wt.% (A), Cr_2O_3 wt.% (B) and CaO wt.% (C) of orthopyroxene from orthopyroxene-rich xenoliths of East Serbia compared with compositions of orthopyroxene of other lithologies of East Serbian upper mantle and those of other localities: 1—East Serbian D/HZ/L xenoliths, 2—Clinopyroxene-rich East Serbian xenoliths related to metasomatism by mafic alkaline melts (Cvetković et al., 2004a), 3—Papua New Guinea (McInnes et al., 2001), 4—Colorado Plateau (Smith et al., 1999), 5—Tallante (Beccaluva et al., 2004), 6— Simcoe Volcanic Field, Washington (Evren Ertan and Leeman, 1996).

orthopyroxene) display lower Mg# and higher but scattered TiO_2 and Na_2O, and very scattered Al_2O_3 and Cr_2O_3 contents in comparison to coarser euhedral clinopyroxene (Type 2) that is unrelated to orthopyroxene relicts. Type 2 clinopyroxene shows uniform Al_2O_3, TiO_2 and Cr_2O_3 wt.% contents and an increase in Na_2O wt.% contents with decreasing Mg#s. In general, OWB_2 clinopyroxene differs from Al-rich clinopyroxene megacrysts, as well as from those formed by reaction with the host (Fig. 4A–D) but overlaps in composition with clinopyroxene occurring in pockets and veins in D/HZ/L xenoliths and with metasomatic clinopyroxene from Patagonian xenoliths.

Spinel from the OWB_2 xenoliths is extremely rich in Cr in comparison to spinels from other mantle xenolith types of East Serbia. Cr#s [$Cr_2O_3/(Cr_2O_3+Al_2O_3)$] are mostly >0.80 with very variable TiO_2 (mostly 1–10 wt. %) contents. There is a compositional difference between interstitial spinel and those included in tabular orthopyroxene. Fig. 5A shows that interstitial spinels display a continuous trend of increasing Ti/Al ratios with decreasing Mg#, whereas spinels included into orthopyroxene remain with very low Ti/Al. In addition, these two spinel types show contrasting trends on the Cr#s vs. Mg# plot (Fig. 5B).

Feldspar is a Na-rich K-feldspar, with an average composition of $An_1Ab_{46}Or_{53}$ and uniform Al_2O_3 and K_2O contents. Na_2O contents are always >5 wt.% and CaO contents are commonly <0.2 wt.%. They are similar to alkali feldspars associated with mantle carbonate described by Delpech et al. (2004) and Chalot-Pratt and Arnold (1999). Carbonate shows a non-uniform Mg-bearing calcite composition with up to 2.6 wt.% MgO and high X_{Ca} [Ca/(Ca+Mg+Fe+Mn)] (>0.93) and Mg# [MgO/(MgO+FeO)] (ranging 0.90–0.97). Ilmenite contains around 52% TiO_2 and 8 wt.% MgO. Four analyses of a single relict pleochroic crystal show good reproducibility but a non-stoichiometric composition. They gave SiO_2 contents around 54 wt.% and Mg#s of 87–90, coupled with ~5 wt.% TiO_2, around 1–1.5 wt.% Al_2O_3, and CaO and Na_2O contents around 5 wt.% and 6 wt.%, respectively. The K_2O and Cr_2O_3 contents are both around 1 wt.%.

5. Trace element contents in minerals

Trace element concentrations were determined on tabular orthopyroxene and interstitial coarser clinopyroxene from coarse-grained OWB_2 xenoliths (Table 3) using laser ablation inductively coupled plasma mass spectrometry (LA-ICP-MS) at the University of Frankfurt. A New Wave Research LUV213™ ultraviolet Nd-YAG laser coupled with a Finnigan MAT ELEMENT2™ was used. The laser was run at a pulse frequency of 10 Hz and a pulse energy of 1.2 mJ for a 150-μm spot size for measurements of orthopyroxene. A spot size of 30 μm and pulse energy of 0.3 mJ was used for clinopyroxene. The USGS BIR 1-G glass (Eggins et

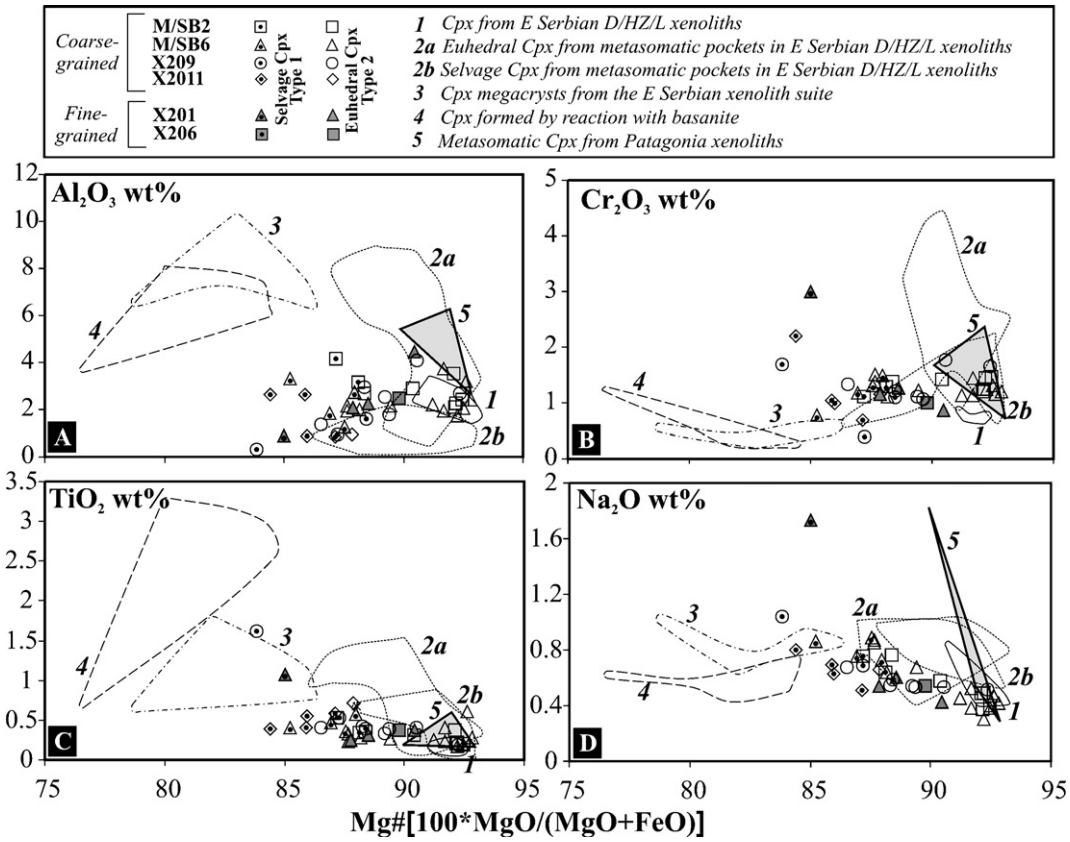

Fig. 4. Plots of Mg# [100*MgO/(MgO+FeO)] vs. Al_2O_3 (A), Cr_2O_3 wt.% (B), TiO_2 wt.% (C), and Na_2O wt.% (D) for clinopyroxene (cpx) occurring in interstitial space of OWB_2 xenoliths; the composition of other clinopyroxene types found in East Serbian xenoliths is also shown (Cvetković et al., 2004a): 1—cpx from the East Serbian D/HZ/L xenoliths, 2—cpx from pockets and veins found in D/HZ/L xenoliths: 2a—coarse and 2b—cpx replacements after orthopyroxene, 3—Al-augite megacrysts, 4—Cpx formed by the reaction with the basanitic host, 5—Metasomatic cpx from the Gobernador Gregores Case, Southern Patagonia (triangles represent three average compositions of Cpx1, Cpx2 and Cpx3 after Laurora et al., 2001).

al., 1997) and NIST612 glass (Pearce et al., 1997) were used as external standards. Silica was used as an internal standard.

OWB_2 orthopyroxene shows uniform but low trace element concentrations. It has a slightly U-shaped pattern on mantle-normalized diagrams with strong peaks at uranium and lead and smaller ones at Rb, Zr and Hf (Fig. 6). The spikes at uranium and lead imply a high oxygen fugacity, and that is in agreement with the estimates of 1–2.4 log(fO_2) relative to the FMQ buffer, reported by Cvetković et al. (2004a). On the other hand, the high concentrations of these elements can be also related to the presence of fluid inclusions in orthopyroxene crystals. The Zr/Hf ratio is constant and lower than the primitive mantle value, with $Zr_N/Hf_N = 0.7–0.8$. Middle rare earth element (MREE) contents are below or close to detection limit, whereas there is a gradual increase of heavy rare earth element (HREE) concentrations from Dy to Lu. OWB_2 orthopyroxene has a similar trace element pattern to those from D/HZ/L xenoliths although with generally higher trace element contents. The pattern is roughly similar to that of orthopyroxene from the Papua New Guinea sub-arc mantle and only differs in lacking the Zr and Y depletions. The OWB_2 orthopyroxene is also more compositionally similar to orthopyroxene from anhydrous xenoliths than to those from hydrous peridotites from SE Spain (Fig. 6).

Nine clinopyroxene grains from two coarse-grained OWB_2 samples and a new analysis of a pocket and vein clinopyroxene from an East Serbian D/HZ/L xenolith are shown on Fig. 7. There is a spectrum of trace element compositions of clinopyroxene. Besides differences between Type 1 and Type 2 clinopyroxenes, which are already distinguished petrographically, some analyses show transitional characteristics, and they are named Type 3 in Fig. 7. Type 1 clinopyroxenes show very low concentrations of most incompatible elements, some below detection limits (e.g. Th, Ta, Hf), and

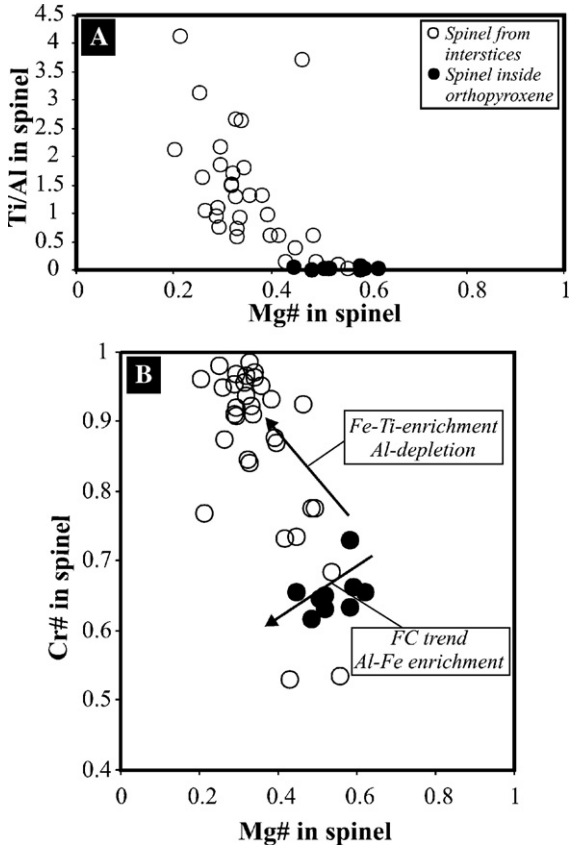

Fig. 5. Mg# [MgO/(MgO+FeO)] vs. Ti/Al (A) and Mg# vs. Cr# [$Cr_2O_3/(Cr_2O_3+Al_2O_3)$] vs. Ti/Al (B) plots for spinels occurring in the East Serbian OWB_2 mantle xenoliths; note an Fe–Al enrichment in primary spinels included in orthopyroxene, which is observed in some cumulates (e.g. Laurent and Kacira, 1987).

relatively high MREE and HREE concentrations. Their mantle-normalized patterns show pronounced spikes at U and Pb and resemble those of the co-existing orthopyroxene (Fig. 7A) but with more than one order of magnitude higher concentrations. Type 1 clinopyroxene is also characterized by low La_N/Ce_N (<1), La_N/Yb_N (<0.7) and Ce_N/Pb_N (<0.5) and high U_N/Nb_N (>3) and Zr_N/Nb_N (>0.7) ratios. Type 2 clinopyroxenes display relatively smooth patterns characterized by enrichment in the most incompatible elements. They show high La_N/Ce_N (>1), La_N/Yb_N (~4) and Ce_N/Pb_N (1.7 and 4.1), coupled with low U_N/Nb_N (~0.5) and Zr_N/Nb_N (<0.3) ratios that are almost an order of magnitude lower than in Type 1. Fig. 8 shows that Type 1 clinopyroxene is similar to clinopyroxenes from the Papuan sub-arc mantle, although the latter are more LREE-enriched. Type 2 clinopyroxene is more akin in composition to East Serbian D/HZ/L and South Patagonia metasomatic clinopyroxenes.

6. Discussion

OWB_2 xenoliths are carbonate- and feldspar-bearing orthopyroxene-rich olivine websterites. Textural evidence suggests that a change in modal composition occurred prior to entrainment. Formation of their present mineral assemblage can be divided into Stage I, when orthopyroxene crystallized, probably with some other phases, and Stage II, when the interstitial minerals formed. To understand the petrogenesis of the OWB_2 mantle lithology and its geodynamic significance, it is necessary to answer three major questions: (1) what processes were responsible for the observed textural disequilibrium?, (2) what was the primary composition of the OWB_2 lithology?, and (3) how did it form within the lithosphere?

6.1. Nature of interstitial patches: evidence from textural relationships and mineral chemistry

Textural evidence shows that all the interstitial minerals, except spinel and maybe some olivine, formed in Stage II. Clinopyroxene regularly replaces orthopyroxene or appears as euhedral/subhedral crystals. These orthopyroxene replacements suggest disequilibrium conditions while the euhedral terminations of coarser clinopyroxene imply rapid and direct precipitation in an open space. The spongy rims suggest a later incomplete resorption of clinopyroxene by an evolved alkali-rich melt. Clinopyroxene is very heterogeneous in major and trace element contents. Consequently, it probably formed shortly before the xenoliths were brought to the surface. Carbonate and K-feldspar clearly crystallized after clinopyroxene. They completely or partially enclose clinopyroxene and the rims of clinopyroxene crystals often show effects of the resorption and/or Al-depletion in contact with K-feldspar (Fig. 2). Textural relationships between carbonate and K-feldspar suggest a co-existence of two immiscible fluids. Apatite and ilmenite crystals almost ubiquitously occur in carbonate and K-feldspar, respectively, but never in clinopyroxene or olivine. This suggests that they crystallized after olivine and clinopyroxene and before carbonate and K-feldspar. In summary, textural evidence establishes the following order of crystallization post-dating orthopyroxene crystallisation: clinopyroxene–apatite+ilmenite–carbonate–K-feldspar.

It is more difficult to discern the time of crystallization of spinel and especially of olivine. Apart from in the interstices, spinel occurs also as inclusion trails and exsolutions in orthopyroxene, suggesting that it formed with orthopyroxene during

Stage I and also during thermal equilibration (exsolution). However, interstitial spinel crystals are more abundant and larger than those within orthopyroxene, indicating that some precipitation of spinel must have also occurred during Stage II. Differences in spinel compositions also argue that spinel crystallization occurred during Stage II, probably as overgrowths and subsolidus change of the composition of primary spinels. Crystallization of olivine during Stage II is suggested by (a) skeletal olivine crystals (Fig. 2D,E,F, G,I), indicating crystallization from an undercooled melt, (b) an intimate relationship with clinopyroxene, suggestive of simultaneous crystallization of these two minerals, (c) textural relationships which imply that crystallization of most interstitial minerals occurred after the alteration of olivine, and (d) Mg# values in olivine, which are less uniform and for some samples slightly higher than Mg# values in orthopyroxene. On the other hand, disintegrated and partially resorbed olivine crystals (Fig. 2G) indicate that the crystallizing melt was not saturated in olivine, at least during some phases of Stage II. Such textural relationships and simultaneous occurrence of skeletal olivines and olivine relicts were reported by Chalot-Pratt and Arnold (1999) in peridotite xenoliths of Romania. They attributed them to the invasion of CO_2-rich fluids and interaction with peridotite. Therefore, some olivine formed probably during Stage I.

From the foregoing discussion the following conclusions may be derived: (a) Stage I was related to formation of tabular orthopyroxene, spinel inclusions and possibly some olivine, (b) exsolution of spinel in orthopyroxene occurred between Stage I and Stage II, and (c) all textural relationships within the interstitial assemblages formed during Stage II. These conclusions can now be used to explain the characteristics and ultimate cause of Stage II processes and to interpret the original composition of these xenoliths.

6.2. Formation of the present interstitial assemblages

If the OWB_2 lithology was originally composed of orthopyroxene, spinel and olivine, then formation of the interstitial minerals must have included addition of other components and/or decomposition of other phases. The small (~100 μm) relicts of a hydrous mineral between orthopyroxene grains suggest that such phases were probably present in the primary OWB_2 lithology. Optical investigations revealed phlogopite characteristics but the electron microprobe data show a composition intermediate between amphibole and phlogopite. The Mg# of the relict mineral is similar to Mg# in the interstitial Fe–Mg phases and in tabular orthopyroxene. Alteration of olivine also implies that H_2O-bearing phases were formerly present and that fluid release occurred due to their decomposition. This alteration cannot be a post-magmatic process because the host rocks contain abundant D/HZ/L xenoliths with fresh olivine. Besides, textural relationships indicate that alteration of olivine occurred before crystallization of feldspar and carbonate.

At this stage it is not possible to determine the composition and modal contribution of hydrous phases. However, similar orthopyroxene-rich mantle domains almost always contain phlogopite and/or amphibole (McInnes and Cameron Eion, 1994; Ertan and Leeman, 1996; Varfalvy et al., 1996; Zanetti et al., 1999; McInnes et al., 2001; Chane-Fo et al., 2003; Beccaluva et al., 2004). Decomposition of hydrous phases has often been documented in mantle xenoliths (Ionov et al., 1994, 1999; Xu et al., 1996, 2000, 2003; Chazot et al., 1996; Neumann and Wulff-Pedersen, 1997; Yaxley et al., 1997; Gorring and Kay, 2000; Laurora et al., 2001; Witt-Eickschen et al., 2003, etc.). Therefore the following discussion is based on the assumption that hydrous minerals were present in the primary OWB_2 lithology.

The present mineral assemblages of interstitial and grain-boundary spaces in between tabular orthopyroxene could have formed (a) by a closed-system process, i.e. solely by decomposition of phases in the original OWB_2 lithology or (b) by an open-system process, with introduction of an external fluid/melt. Closed-system decomposition of H_2O-bearing phases is usually attributed to decompression melting or increased temperature upon the entrapment of xenoliths by a hot magma (e.g. Chazot et al., 1996; Yaxley et al., 1997). However, disequilibrium textures and the presence of carbonate suggest the role of an external agent which was not in equilibrium with orthopyroxene, i.e. that the system was not closed. Mg-calcite is stable above 1–1.6 GPa at 860–1020 °C (e.g. Dalton and Wood, 1993). Mass-balance calculations also do not support a closed-system process. The average bulk chemical composition of the present interstitial assemblages could not be obtained by any possible mixture of orthopyroxene, hypothetical phlogopite, amphibole and carbonate. Thus, a closed-system process is unlikely and formation of the interstices must be explained by an alternative mechanism.

Decomposition of hydrous mantle phases by infiltration of metasomatic fluids/melts has been described by Ionov et al. (1994). To test the hypothesis that the present interstitial mineral assemblages of the OWB_2

Table 3
LA-ICP-MS trace element analyses of orthopyroxene and clinopyroxene from East Serbian OWB2 xenoliths and an analysis of clinopyroxene from metasomatic pockets and veins found in D/HZ/L xenoliths (Cpx P&V)

ppm	Orthopyroxene								
	M/SB2				M/SB6				
	Opx-1	Opx-2	Opx-3	Opx-4	Opx-1	Opx-2	Opx-3	Opx-4	Opx-5
Li	23.56	18.92	14.72	14.72	27.29	14.77	24.77	15.69	5.68
B	n.a.	n.a.	n.a.	n.a.	n.a.	n.a.	n.a.	n.a.	n.a.
Sc	14.93	15.14	15.37	15.15	15.32	15.30	16.18	17.12	15.95
V	n.a.	n.a.	n.a.	n.a.	n.a.	n.a.	n.a.	n.a.	n.a.
Cr	3726.8	3923.0	3836.8	3458.3	3717.8	3734.1	3546.0	3835.0	4005.0
Mn	1426.3	1424.6	1453.7	1452.0	1325.0	1363.3	1372.4	1415.6	1406.4
Co	n.a.	n.a.	n.a.	n.a.	n.a.	n.a.	n.a.	n.a.	n.a.
Ni	793.3	793.5	792.0	790.7	735.4	747.9	787.1	766.0	793.2
Cu	n.a.	n.a.	n.a.	n.a.	n.a.	n.a.	n.a.	n.a.	n.a.
Zn	n.a.	n.a.	n.a.	n.a.	n.a.	n.a.	n.a.	n.a.	n.a.
Rb	0.03	0.20	0.02	0.01	0.05	0.12	0.04	0.06	0.10
Sr	0.097	0.409	0.130	0.049	0.790	0.222	0.515	0.454	0.328
Y	0.134	0.181	0.160	0.126	0.438	0.142	0.346	0.316	0.251
Zr	0.913	0.969	1.427	0.580	1.032	1.315	0.900	1.890	1.123
Nb	0.032	0.066	0.033	0.014	0.049	0.067	0.011	0.034	0.065
Cs	n.a.	n.a.	n.a.	n.a.	n.a.	n.a.	n.a.	n.a.	n.a.
Ba	0.098	0.862	0.068	0.029	0.350	0.897	0.235	0.184	0.341
La	0.012	0.014	0.016	0.008	0.036	0.014	0.024	0.034	0.022
Ce	0.020	0.027	0.026	0.010	0.098	0.020	0.062	0.065	0.042
Pr	0.003	0.005	b.d.l.	0.003	0.012	0.004	0.008	0.006	0.005
Nd	0.037	b.d.l.	b.d.l.	b.d.l.	0.049	b.d.l.	0.036	0.030	0.024
Sm	b.d.l.	b.d.l.	b.d.l.	b.d.l.	0.026	b.d.l.	0.026	0.020	b.d.l.
Eu	b.d.l.	b.d.l.	b.d.l.	b.d.l.	0.007	0.005	0.007	0.007	b.d.l.
Gd	b.d.l.	b.d.l.	b.d.l.	b.d.l.	0.038	b.d.l.	0.022	0.019	0.026
Tb	b.d.l.	b.d.l.	b.d.l.	b.d.l.	0.007	b.d.l.	0.008	b.d.l.	0.003
Dy	b.d.l.	0.036	b.d.l.	0.027	0.077	0.016	0.051	0.048	0.043
Ho	0.005	0.009	b.d.l.	b.d.l.	0.017	0.008	0.016	0.013	0.010
Er	0.035	0.029	0.020	0.016	0.061	0.036	0.047	0.040	0.047
Tm	0.006	0.006	0.007	0.006	0.011	0.006	0.009	0.009	0.007
Yb	0.050	0.058	0.058	0.056	0.083	0.051	0.077	0.061	0.060
Lu	0.012	0.012	0.016	0.013	0.018	0.013	0.019	0.019	0.013
Hf	0.034	0.032	0.046	0.023	0.037	0.044	0.028	0.060	0.038
Ta	b.d.l.	0.003	b.d.l.	b.d.l.	b.d.l.	0.002	b.d.l.	0.003	b.d.l.
Pb	0.062	0.387	0.630	0.085	0.074	0.048	0.570	0.180	0.208
Th	0.019	0.023	0.019	0.035	0.020	0.026	0.018	0.020	0.019
U	0.091	0.076	0.176	0.037	0.069	0.162	0.071	0.224	0.117

ppm	Clinopyroxene									
	M/SB2				M/SB6					P&V
	Cpx-1	Cpx-2	Cpx-3	Cpx-4	Cpx-1	Cpx-2	Cpx-3	Cpx-4	Cpx-5	Cpx-1
Li	6.3	26.3	5.9	8.1	35.1	25.2	13.0	9.9	12.3	39.7
B	3.6	4.3	4.0	4.7	3.5	3.1	4.1	3.6	3.4	5.1
Sc	96.9	116	94.5	92.6	111	89.6	84.6	101	107	93.6
V	518	533	387	362	400	274	233	334	328	281
Cr	11120	9117	9369	11539	n.a.	n.a.	n.a.	n.a.	n.a.	n.a.
Mn	997.3	1011	939.2	971.2	1616	1136	1575	1482	1944	1965
Co	38.8	39.0	40.1	28.1	33.2	29.7	29.7	22.6	31.4	74.6
Ni	866	710	822	557	572	919	653	509	651	1771
Cu	5.3	11.7	10.8	9.0	9.3	7.2	63.1	6.7	5.3	206.8
Zn	38.3	25.3	28.7	20.6	24.6	15.8	31.4	21.2	30.3	103.5
Rb	1.00	0.80	3.88	11.05	1.93	0.19	2.89	19.22	1.65	1.22

Table 3 (*continued*)

ppm	Clinopyroxene									
	M/SB2				M/SB6					P&V
	Cpx-1	Cpx-2	Cpx-3	Cpx-4	Cpx-1	Cpx-2	Cpx-3	Cpx-4	Cpx-5	Cpx-1
Sr	15.2	17.3	98.2	53.6	45.0	7.86	127.1	79.6	118.0	208.1
Y	8.71	9.37	9.44	8.60	11.17	6.23	9.71	11.55	9.36	10.72
Zr	4.05	3.25	6.78	9.05	12.19	1.88	27.75	28.83	8.84	39.18
Nb	0.31	0.27	1.14	4.74	7.36	0.09	11.99	5.70	0.84	7.93
Cs	b.d.l.	0.04	0.05	0.06	b.d.l.	b.d.l.	0.09	0.04	0.04	0.14
Ba	3.7	7.5	19.5	28.0	8.4	1.2	46.2	35.2	7.3	11.0
La	1.21	0.23	1.24	2.59	1.29	0.11	5.96	6.73	1.59	8.95
Ce	3.15	0.81	3.40	6.92	3.50	0.43	15.00	15.54	4.65	20.79
Pr	0.37	0.11	0.47	0.84	0.43	0.07	1.93	1.81	0.62	2.82
Nd	1.6	0.9	1.8	3.6	2.2	b.d.l.	8.8	7.2	2.7	12.8
Sm	b.d.l.	0.5	0.9	1.1	0.8	b.d.l.	2.0	1.4	0.6	3.0
Eu	0.2	0.3	0.3	0.2	0.3	b.d.l.	0.7	0.5	0.3	0.9
Gd	0.8	1.1	1.0	1.1	0.8	0.5	2.2	1.5	1.1	2.5
Tb	0.14	0.16	0.19	0.15	0.19	b.d.l.	0.25	0.29	0.16	0.33
Dy	1.4	1.5	1.7	1.5	2.0	1.1	1.9	2.0	1.6	2.2
Ho	0.36	0.35	0.35	0.30	0.42	0.35	0.41	0.45	0.35	0.48
Er	1.21	1.30	0.95	1.01	1.40	0.81	0.86	1.18	0.95	1.26
Tm	0.16	0.21	0.20	0.13	0.25	0.14	0.08	0.21	0.19	0.18
Yb	1.2	1.2	1.4	1.3	1.5	0.8	0.9	1.3	1.1	0.9
Lu	0.20	0.19	0.23	0.18	0.16	0.13	0.17	0.24	0.19	0.13
Hf	b.d.l.	b.d.l.	0.2	b.d.l.	0.3	b.d.l.	1.0	0.8	b.d.l.	0.9
Ta	0.1	b.d.l.	0.0	0.2	0.4	b.d.l.	0.5	0.4	0.1	0.6
Pb	0.6	1.4	1.0	2.0	0.4	1.3	0.8	0.3	0.3	3.0
Th	b.d.l.	b.d.l.	0.2	0.3	0.4	b.d.l.	0.7	0.7	0.2	1.0
U	b.d.l.	0.04	0.15	0.10	0.06	0.03	0.21	0.06	0.27	0.83

xenoliths were formed by similar processes, we have to constrain the possible composition and modal contribution of hydrous phases, on one side, and of the metasomatic agent, on the other. We have estimated the modal abundance of the hydrous phases on the basis of water content in phyllosilicates related to alteration of

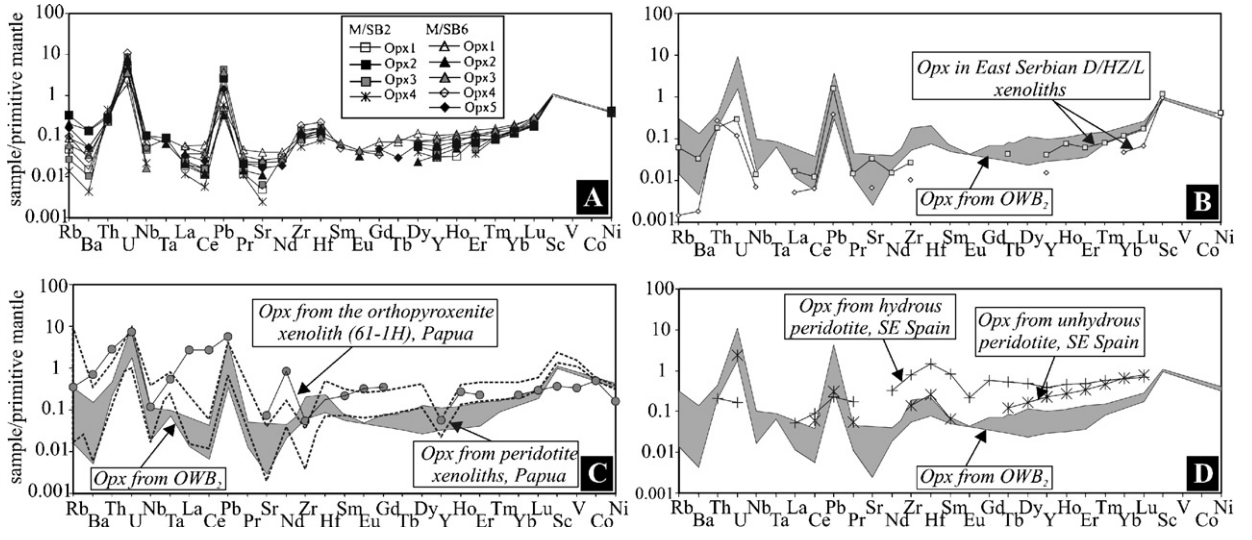

Fig. 6. (A) Primitive mantle-normalized (McDonough and Sun, 1995) multielement diagram for orthopyroxenes in the East Serbian OWB_2 xenolith suite compared to compositions of orthopyroxene in the 'normal mantle' underneath East Serbia (Cvetković et al., 2004a) (B), orthopyroxene from Papua New Guinea xenoliths (Gregoire et al., 2001) (C), and orthopyroxene of Tallante SE Spain xenoliths (Beccaluva et al., 2004) (D).

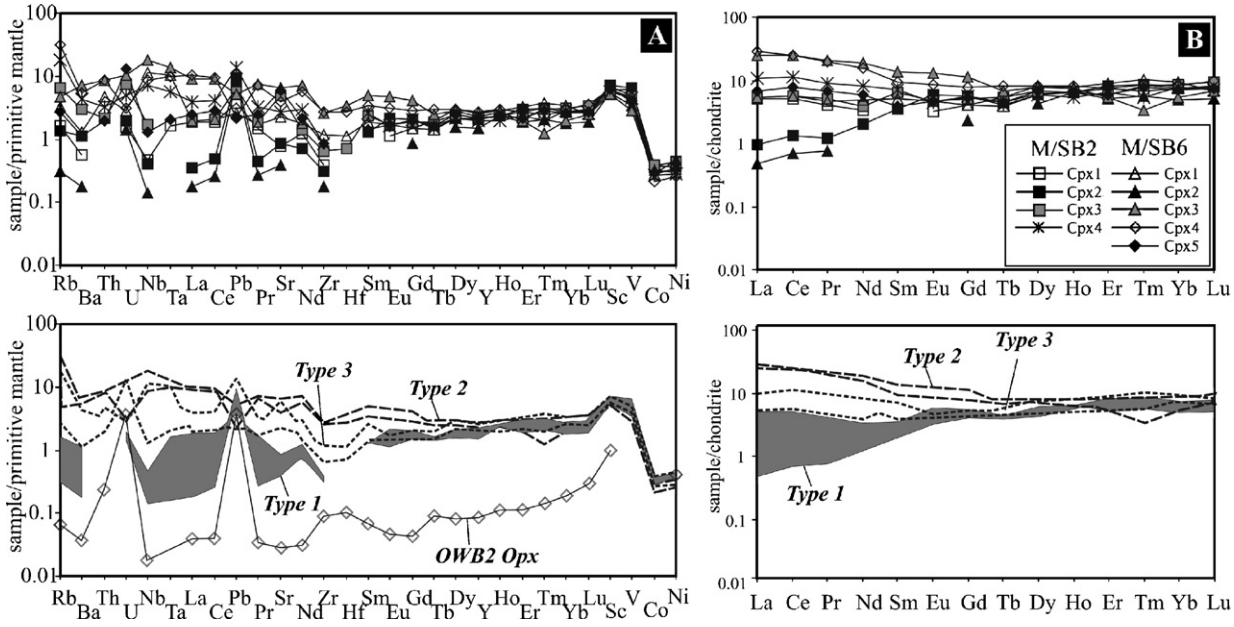

Fig. 7. Primitive mantle-normalized (McDonough and Sun, 1995) multielement diagram (A) and chondrite-normalized REE diagram (B) for Types 1, 2 and 3 of clinopyroxene in the East Serbian OWB_2 xenolith suite; the composition of a representative OWB_2 orthopyroxene is also given for comparison.

olivine, assuming that all this water came from the previous H_2O-bearing minerals. Given the amount of altered olivine of ~15 vol.% (average volume of interstitial patches) and that the water content of the phyllosilicates is ~13 wt.%, we obtain a bulk water content of the interstices of around 2 wt.%. This estimate accounts for a maximum total envisaged amphibole–phlogopite abundance of 60 vol.% (assuming an average H_2O content of the amphibole–phlogopite mixture of 3 wt.%).

However, such a high modal content of hydrous minerals is ruled out by results of mass balance calculations (Table 4). An average modal interstitial assemblage of 0.37[ol]+0.11[cpx_{Type1}]+0.24[cpx_{Type2}]+0.17[K-f]+0.07[Mg-cc]+0.02[Ti-rich sp]+0.01[ap]+0.01[ilm] is balanced with 0.56[opx]+0.15[phl]+0.12[amph]+0.01[Ti-poor sp]+0.16[low silica, high-CaO, high-CO_2 fluid/melt]. In the calculations we used microprobe analyses of present minerals, a Ti-Cr rich phlogopite from Serbian primitive lamproites (Prelević et al., 2005) and an amphibole from Finero websterite (Zanetti et al., 1999) and we assumed that all olivine is metasomatic. The calculations assuming that half of the olivine was originally present produced the following reaction: 0.2[ol]+0.14[cpx_{Type1}]+0.31[cpx_{Type2}]+0.21[K-f]+0.085[Mg-cc]+0.025[Ti-rich sp]+0.015[ap]+0.015[ilm]=0.41[opx]+0.10[phl]+0.11[amph]+0.01[Ti-poor sp]+0.37[CO_2-rich, Al_2O_3-poor alkaline fluid/melt]. These calculations show that reaction between orthopyroxene, hydrous phases and an external metasomatic agent could have produced the observed minerals within the interstitial patches in both cases. However, the model in which olivine was already present requires a smaller contribution of orthopyroxene and phlogopite and a higher amount of metasomatic agent. In the first case, the metasomatic agent was similar to a calciocarbonatite, and in the second was more akin to a highly CO_2-rich alkaline mafic melt.

It is unlikely that infiltration of the host magma caused Stage II. This is ruled out by (a) textural relationships (sharp contacts towards the host basanites, absence of interconnected veins, etc.), (b) composition of metasomatic clinopyroxene that is different from clinopyroxene texturally related to the host, and (c) the mass-balance calculations. In addition, decomposition of phlogopite at high pressures and under CO_2-rich conditions has been studied experimentally by Wendlandt and Eggler (1980). If crystallization of OWB_2 metasomatic clinopyroxene was related to infiltration of the host magma, then Mg# values in the clinopyroxene had to be buffered by OWB_2 orthopyroxene which was involved in the reaction. However, lower Mg#s were observed in clinopyroxene selvages around partially dissolved orthopyroxene than in euhedral clinopyroxene directly crystallized from the melt. Moreover, OWB_2 clinopyroxene has a similar trace element pattern to

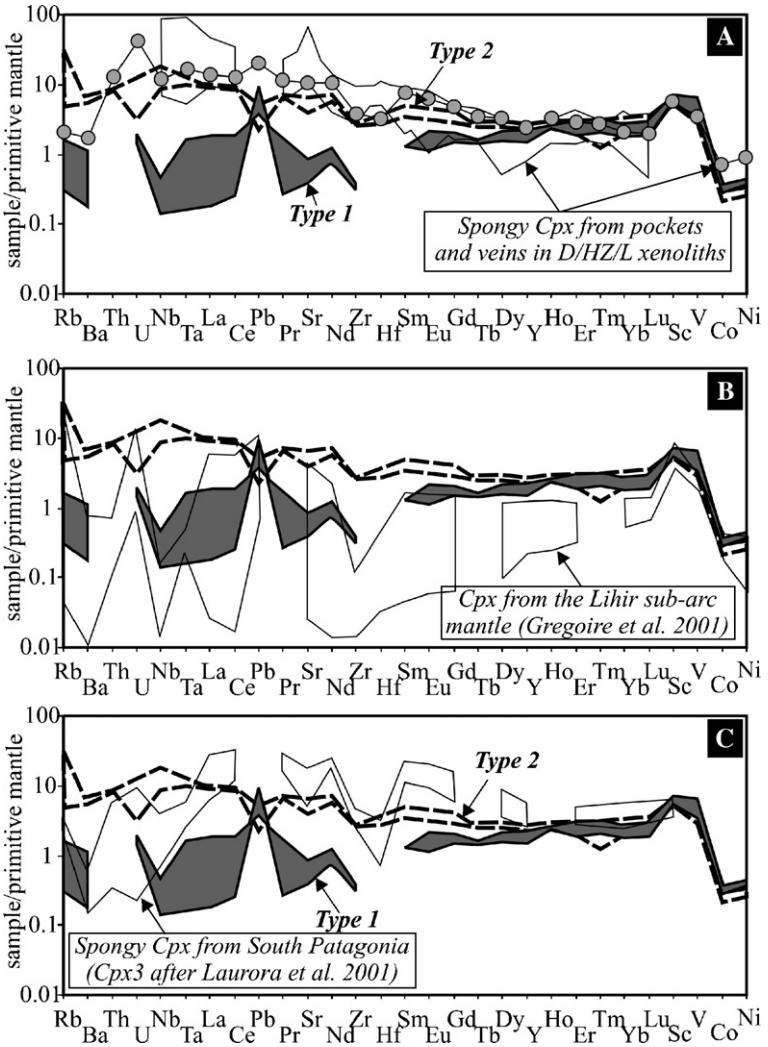

Fig. 8. Primitive mantle-normalized (McDonough and Sun, 1995) multielement diagrams for Type 1 and Type 2 OWB_2 clinopyroxene compared with the composition of (A) spongy clinopyroxene occurring in pockets and veins of East Serbian D/HZ/L xenoliths (Cvetković et al., 2004a, this study), (B) clinopyroxene from the sub-arc mantle of Papua New Guinea (Gregoire et al., 2001), and (C) spongy clinopyroxene in metasomatic pocket assemblages from South Patagonian xenoliths (Laurora et al., 2001).

metasomatic clinopyroxene in pockets and veins in East Serbian D/HZ/L and South Patagonian xenoliths, both of which have been attributed to metasomatism (Laurora et al., 2001; Cvetković et al., 2004a).

In order to further characterize the composition of the metasomatic agent, we have performed a calculation of its trace element contents using the chemical composition of Type 2 clinopyroxene and partition coefficients of Downes et al. (2004). In Fig. 9 the pattern of the calculated liquid is compared to that of the basanitic host (Cvetković et al., 2004b). They have similar REE contents, but show differences in Ba, Nb, Hf and Zr contents. This suggests that the hypothetical liquid may have been highly incompatible element-enriched mafic alkaline magma with addition of a CO_2-, LREE- and LILE-enriched component.

Summarizing, the observed mineral phases and textural relationships are interpreted to have formed at the expense of already present amphibole, phlogopite and orthopyroxene by melting induced by infiltration of calciocarbonatitic or CaO- and CO_2-rich silicate melt.

6.3. The primary nature and origin of OWB_2 xenoliths

The evidence presented above suggests that the original OWB_2 lithology was a hydrous olivine-bearing orthopyroxenite. Mass balance calculations suggest that orthopyroxene accounted for about 50 vol.% of the

Table 4

Minerals presently occurring within the interstices									Hypothetical reaction assemblage					
Mineral	OL	CPX1	CPX2	KF	CC	Ti-rich Sp	Ap	Ilm	Mineral	OPX	PHL	AMPH	Ti-poor SP	MA
Results of mass-balance calculation of the possible formation of OWB2 interstitial assemblages (total present olivine produced in Stage II)														
% vol	0.370	0.110	0.240	0.170	0.070	0.020	0.010	0.010	% vol	0.560	0.150	0.120	0.010	0.160
SiO_2, wt%	40.07	53.44	51.90	65.48	0.01	0.47		0.45	SiO_2, wt%	55.95	40.70	46.00	0.05	8.80
TiO_2	0.02	0.36	0.41	0.04	0.00	4.33		52.87	TiO_2	0.04	2.50	0.67	0.45	1.90
Al_2O_3	0.03	1.28	3.75	19.65	0.00	4.56		0.17	Al_2O_3	1.40	12.90	11.71	17.01	1.80
FeO	10.38	4.46	2.97	0.06	0.13	34.55		33.80	FeO	8.23	4.80	3.55	21.97	0.20
MnO	0.18	0.19	0.06	0.03	0.11	3.79		0.44	MnO	0.18	0.10	0.09	0.31	0.20
MgO	49.21	18.39	18.71	0.01	2.61	6.93	1.48	7.95	MgO	32.69	22.90	19.00	12.68	6.00
CaO	0.19	18.65	19.53	0.05	58.31	0.23	51.97	0.12	CaO	0.54	0.10	11.49	0.01	60.00
Na_2O	0.02	0.89	0.52	5.91	0.00		0.91		Na_2O	0.01	0.30	2.76		5.00
K_2O	0.00	0.01	0.01	8.36	0.05		42.48		K_2O	0.00	9.90	0.84		1.50
Cr_2O_3	0.06	1.30	1.44	0.00	0.00	45.69		2.16	Cr_2O_3	0.25	1.50	2.00	48.25	2.20
Results of mass-balance calculation of the possible formation of OWB2 interstitial assemblages (half of present olivine produced in Stage II)														
% vol	0.200	0.140	0.310	0.210	0.085	0.025	0.015	0.015	% vol	0.410	0.100	0.110	0.005	0.375
SiO_2, wt%	40.07	53.44	51.90	65.48	0.01	0.47	0.45		SiO_2, wt%	55.98	40.70	46.00	0.05	35.30
TiO_2	0.02	0.36	0.41	0.04	0.00	4.33		52.87	TiO_2	0.04	2.50	0.67	0.45	2.00
Al_2O_3	0.03	1.28	3.75	19.65	0.00	4.56		0.17	Al_2O_3	1.40	12.90	11.71	17.01	6.50
FeO	10.38	4.46	2.97	0.06	0.13	34.55		33.80	FeO	8.23	4.80	3.55	21.97	1.60
MnO	0.18	0.19	0.06	0.03	0.11	3.79		0.44	MnO	0.18	0.10	0.09	0.31	0.20
MgO	49.21	18.39	18.71	0.01	2.61	6.93	1.480	7.95	MgO	32.69	22.90	19.00	12.68	2.40
CaO	0.19	18.65	19.53	0.05	58.31	0.23	51.97	0.12	CaO	0.54	0.10	11.49	0.01	34.50
Na_2O	0.02	0.89	0.52	5.91	0.00		0.91		Na_2O	0.01	0.30	2.76		3.01
K_2O	0.00	0.01	0.01	8.36	0.05		42.48		K_2O	0.00	9.90	0.84		3.30
Cr_2O_3	0.06	1.30	1.44	0.00	0.00	45.69		2.16	Cr_2O_3	0.25	1.50	2.00	48.25	2.90

present interstitial spaces. The maximum amount of hydrous phases is estimated to be around 6 vol.% of the total rock volume and that indicates that a negligible amount of H_2O (~0.2 wt.%) was originally present in the OWB_2 lithology.

Recent studies have demonstrated that orthopyroxene-rich mantle rocks may originate by (a) deserpentinization in the upper mantle (Arai and Kida, 2000; Arai et al., 2003), (b) metasomatic reactions between peridotite and percolating melts/fluids (McInnes and Cameron Eion, 1994; Kelemen et al., 1995; Ertan and Leeman, 1996; Smith, 1997; Smith et al., 1999; Gregoire et al., 2001; McInnes et al., 2001; Chane-Fo et al., 2003), or (c) direct crystallization from a melt saturated in orthopyroxene (Varfalvy et al., 1996; Al-Boghdady and Economou-Eliopoulos, 2005). Our data

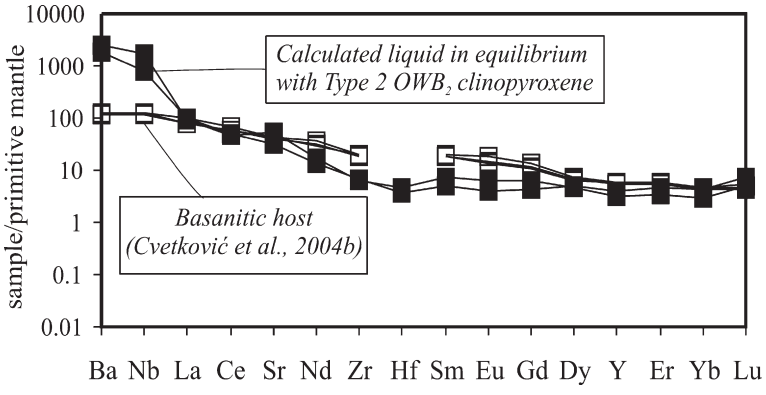

Fig. 9. Primitive mantle-normalized multielement pattern for the calculated composition of liquid in equilibrium with OWB_2 clinopyroxene of Type 2 compared to the pattern of the host basanites (Cvetković et al., 2004b). In the calculations $^{Cpx/Lq}D$ values of Downes et al. (2004) were used.

do not support an origin for OWB_2 xenoliths by processes (a) and (b). This is inferred from textural relationships (e.g. cumulitic texture instead of fibrous orthopyroxene aggregates or porphyroblasts, presence of spinel exsolution and absence of olivine inclusions in orthopyroxene) and mineral composition (e.g. lower LREE and LILE contents in OWB_2 orthopyroxene in comparison to metasomatic orthopyroxene from Papuan and SE Spanish orthopyroxene-rich xenoliths). The Mg#s in OWB_2 orthopyroxene are markedly lower (~86) than Mg#s in orthopyroxene from the East Serbian 'normal mantle' and metasomatic fibrous orthopyroxene of the Papuan xenoliths (Fig. 3). This suggests that Mg#s of OWB_2 orthopyroxene were not buffered by the peridotite but, more probably, by the magma from which the orthopyroxene crystallized. In addition, differences in Mg# in orthopyroxene from coarse- and fine-grained samples imply the role of fractional crystallization.

It is difficult to establish the true composition of the magma from which the OWB_2 primary assemblage crystallized, because: (1) the primary OWB_2 petrography may not reflect a liquid composition but crystal accumulation, and (2) the composition was further changed by Stage II. Early crystallization of orthopyroxene indicates silica-saturated or oversaturated melts (e.g. Kushiro, 1969; Morse, 1980), i.e. magmas with >53 wt.% SiO_2. Using the $^{Fe-Mg}Kd_{opx}$ ($^{Fe-Mg}Kd_{opx} = [FeO_{opx}MgO_{liq}/FeO_{liq}MgO_{opx}]$) of 0.27 (Kinzler and Grove, 1992), we calculated Mg# up to 0.65 for liquids in equilibrium with OWB_2 orthopyroxene. Taking fractionation into account, the OWB_2 primary melts could have had ~54–55 wt.% SiO_2 and Mg#>0.65. These characteristics are comparable to high-Mg andesites (e.g. Wang et al., 2002) and boninites (e.g. Hickey and Frey, 1982).

6.4. Possible geodynamic constraints

East Serbian OWB_2 xenoliths initially formed as orthopyroxenite mantle rocks. Similar orthopyroxene-rich mantle material has been found in Papua New Guinea (Gregoire et al., 2001; McInnes et al., 2001), SE Spain (Beccaluva et al., 2004), NW USA (Brandon and Draper, 1996; Ertan and Leeman, 1996), Kamchatka (Arai et al., 2003), British Columbia (Chane-Fo et al., 2003), Colorado (Smith, 1997; Smith et al., 1999), Southern Andes (Kilian et al., 1999), Philippines (Arai and Kida, 2000), Finero peridotite (Zanetti et al., 1999), Pindos ophiolite (Al-Boghdady and Economou-Eliopoulos, 2005), Bay of Island ophiolite (Varfalvy et al., 1996), Zabargard peridotite (Schmidt et al., 2000), and Cabo Ortegal peridotite (Santos et al., 2002). Most of these areas have a close spatial and temporal relation to subduction. The existence of OWB_2 xenoliths is coupled with a strongly depleted signature of the regional lithospheric mantle, which also suggests a supra-subduction zone setting (Cvetković et al., in preparation). Experimental data have shown that the Fe-Mg equilibration between melts and surrounding mantle is relatively fast (Hirose and Kushiro, 1993). Although the rate of Fe–Mg equilibration would depend on the size of the orthopyroxenite cumulates, the contrast in Fe–Mg distribution between the OWB_2 silicates and those from D/HZ/L xenoliths suggests that these orthopyroxenite domains did not reside long in the mantle before they were captured by basanitic magma. This means that if these orthopyroxenites originated by subduction, the most likely candidate is the Mesozoic subduction related to closure of the Tethyan ocean (Karamata and Đorđević, 1980; Cioflica et al., 1995; Karamata et al., 1997, 1999; Ciobanu et al., 2002).

This study has shown that the original orthopyroxenite lithology was changed by metasomatism. The metasomatic agents ranged in composition from CO_2-rich silica-undersaturated mafic alkaline melts to silica-poor, highly CaO- and CO_2-rich fluids. The role of mafic alkaline metasomatism within the regional lithosphere has been documented by Cvetković et al. (2004a). This was explained in terms of very small degree melts from the same asthenospheric source which later formed the host basanitic magma. Pockets and veins in D/HZ/L xenoliths were interpreted to have originated in this way. The role of calciocarbonatitic fluids appears to be much more evident in OWB_2 xenoliths. Mantle carbonates may be formed by subduction (Maury et al., 1992; Szabo et al., 1996; Demeny et al., 2004). In the frame of the model proposed below we speculate that the OWB_2 carbonates could be related to earlier subduction.

Thus, during the Late Cretaceous, the East Serbian lower lithosphere was a mantle wedge above a subduction zone. Convergence caused closure of the western branch of the Vardar Zone and subduction formed Late Cretaceous calc-alkaline magmatism. During subduction, in the fore-arc region of the mantle wedge, SiO_2-saturated, boninite-like magmas were formed due to a high H_2O-flux into a refractory harzburgitic mantle. These magmas precipitated as hydrous olivine-bearing orthopyroxenite bodies (primary OWB_2 lithology, Stage I). At the same time, other subduction components, particularly CO_2-rich fluids, were also introduced into the fore-arc lithospheric mantle, leading to precipitation of Mg-

carbonate. After subduction ceased, this lithosphere was subjected to much higher heat flow, when mafic alkaline magmatism occurred in the Palaeogene. Small degree alkaline melts, as precursors to this magmatism, metasomatized the lower lithosphere and formed metasomatic pockets and veins in the D/HZ/L mantle. A possible scenario may be that some of these alkaline melts came into contact with previously precipitated carbonates, and hybrid metasomatic agents of a wide range of compositions between alkaline mafic melts and calciocarbonatitic fluids were produced. Incorporation of a carbonatitic component decreased the viscosity of these hybrid fluids and enabled them to percolate to shallower lithospheric levels, leading to interaction with the orthopyroxenite bodies (Stage II). This gave rise to decomposition of hydrous minerals, partial dissolution of orthopyroxene and formation of the interstitial assemblage in OWB_2 xenoliths.

7. Conclusions

Carbonate- and feldspar-bearing olivine websterite xenoliths provide evidence of two-stage processes of modification in the lithospheric mantle beneath East Serbia. These rocks primarily were orthopyroxenites with small amounts of olivine, hydrous minerals and spinel. They formed by fractionation of a SiO_2-saturated, high-Mg primary magma formed by H_2O flux-induced melting of a highly refractory mantle. This lithospheric magmatism most probably occurred within the fore-arc mantle wedge during Mesozoic subduction. Prior to entrapment in the host alkaline magma this orthopyroxenite lithology was exposed to metasomatic processes during which dissolution of orthopyroxene, decomposition of primary hydrous minerals and formation of present interstitial mineral assemblages occurred. This metasomatism was an immediate precursor to the host mafic alkaline magmatism, the effects of which have already been observed in other lithologies in the regional mantle.

Acknowledgement

This study was supported by the Royal Society (UK) and by a Lise Meitner Fellowship granted to V. Cvetković by the Austrian Science Foundation (M832 N10). VC and DP thank the Ministry of Science and Environment Protection and Serbian Academy of Science and Arts, Geodynamics Project, for support. ML thanks the Karađorđević Royal Family Fund for financial support and the Institute of Mineralogy, University of Frankfurt, for EPMA and LA-ICP-MS analyses. Thoughtful and constructive reviews were provided by two anonymous referees. Careful editorial comments of S. Foley led to a significant improvement of the paper.

References

Al-Boghdady, A., Economou-Eliopoulos, M., 2005. Fluid inclusions in chromite from a pyroxenite dyke of the Pindos ophiolite complex. Chemie der Erde Geochemistry 65 (2), 191–202.

Arai, S., Kida, M., 2000. Origin of fine-grained peridotite xenoliths from Iraya volcano of Batan Island, Philippines: deserpentinization or metasomatism at the wedge mantle beneath an incipient arc? Island Arc 9, 458–471.

Arai, S., Ishimaru, S., Okrugin, V., 2003. Metasomatized harzburgite xenoliths from Avacha volcano as fragments of mantle wedge of the Kamchatka arc: implication for the metasomatic agent. Island Arc 12, 233–246.

Beccaluva, L., Bianchini, G., Bonadiman, C., Siena, F., Vaccaro, C., 2004. Coexisting anorogenic and subduction-related metasomatism in mantle-xenoliths from the Betic Cordillera (southern Spain). Lithos 75, 67–87.

Berza, T., Constantinescu, E., Vlad, S., 1998. Upper Cretaceous magmatic series and associated mineralisation in the Carpathian-Balkan Orogen. SRG-SEG Joint Symposium on Granite Types and Mineralization, vol. 48. Society of Resource Geology, Tokyo, Japan, pp. 291–306.

Brandon, A.D., Draper, D.S., 1996. Constraints on the origin of the oxidation state of mantle overlying subduction zones: An example from Simcoe, Washington, USA. Geochemical Journal 60 (10), 1739–1749.

Chalot-Pratt, F., Arnold, M., 1999. Immiscibility between calciocarbonatitic and silicate melts and related wall rock reactions in the upper mantle: a natural case study from Romanian mantle xenoliths. Lithos 46, 627–657.

Chane-Fo, I., Godard, M., Tommasi, A., Vauchez, A., Belley, F., Lapierre, H., Tardy, Y., 2003. Partial melting and melt circulation above a subduction zone: a petrophysical and geochemical study of the refractory peridotites and pyroxenites from Murray Ridge, British Columbia. Geophysical Research Abstracts 5, 11289.

Chazot, G., Menzies, M.A., Harte, B., 1996. Determination of partition coefficients between apatite, clinopyroxene, amphibole, and melt in natural lherzolites from Yemen: implications for wet melting in the lithospheric mantle. Geochimica et Cosmochimica Acta 60, 423–437.

Ciobanu, C., Cook, N.J., Stein, H., 2002. Regional setting and geochronology of the Late Cretaceous Banatitic Magmatic and Metallogenetic Belt. Mineralium Deposita 37, 541–567.

Cioflica, G., Jude, R., Lupulescu, M., Palaseanu, M., 1995. Late Cretaceous-Eocene arc magmatism in the western part of the South Carpathians, Romania. Proceedings of the XV congress of the Carpatho-Balkan Geological Association. Geological Society of Greece, vol. 4, pp. 495–500.

Cvetković, V., Downes, H., Prelević, D., Jovanović, M., Lazarov, M., 2004a. Characteristics of the lithospheric mantle beneath East Serbia inferred from ultramafic xenoliths in Palaeogene basanites. Contributions to Mineralogy and Petrology 148, 335–357.

Cvetković, V., Prelević, D., Downes, H., Jovanović, M., Vaselli, O., Pecskay, Z., 2004b. Origin and geodynamic significance of

Tertiary post-collisional basaltic magmatism in Serbia (central Balkan Peninsula). Lithos 73/3-4, 161–186.

Dalton, J.A., Wood, B.J., 1993. The partitioning of Fe and Mg between olivine and carbonate and the stability of carbonate under mantle conditions. Contributions to Mineralogy and Petrology 114, 501–509.

Delpech, G., Gregoire, M., O.Reilly, S.Y., Cottin, J.Y., Moine, B., MIchon, G., Giret, A., 2004. Feldspar from carbonate-rich silicate metasomatism in the shallow oceanic mantle under Kerguelen Islands (South Indian Ocean). Lithos 75, 209–237.

Demeny, A., Vennemann, T.W., Hegner, E., Nagy, G., Milton, J.A., Embey-Isztin, A., Homonnay, Z., Dobosi, G., 2004. Trace element and C–O–Sr–Nd isotope evidence for subduction-related carbonate-silicate melts in mantle xenoliths (Pannonian Basin, Hungary). Lithos 75, 89–113.

Downes, H., 2001. Formation and modification of the shallow subcontinental lithospheric mantle: evidence from ultramafic xenoliths suites and massifs of western and central Europe. Journal of Petrology 42, 233–250.

Downes, H., Vaselli, O., Seghedi, I., Ingram, G., Rex, D., Coradossi, N., Pecskay, Z., Pinarelli, L., 1995. Geochemistry of late Cretaceous–early Tertiary magmatism in Poiana Rusca (Romania). Acta Vulcanologica 7, 209–217.

Downes, H., Beard, A., Hinton, R., 2004. Natural experimental charges: an ion-microprobe study of trace element distribution coefficients in glass-rich hornblendite and clinopyroxenite xenoliths. Lithos 75, 1–17.

Eggins, S.M., Woodhead, J.D., Kinsley, L.P.J, Mortimer, G.E., Sylvester, P., McCulloch, M.T., Hergt, J.M., Handler, M.R., 1997. A simple method for the precise determination of >40 trace elements in geological sample by ICPMS using enriched isotope internal standardization. Chemical Geology 134, 311–326.

Embey-Isztin, A., Dobosi, G., Altherr, R., Meyer, H.P., 2001. Thermal evolution of the lithosphere beneath the western Pannonian Basin; evidence from deep-seated xenoliths. Tectonophysics 331 (3), 285–306.

Ertan, I.E., Leeman, W.P., 1996. Metasomatism of Cascades subarc mantle: evidence from a rare phlogopite orthopyroxenite xenolith. Geology 24 (5), 451–454.

Frey, F.A., Prinz, M., 1978. Ultramafic inclusions from San Carlos, Arizona: petrologic and geochemical data bearing on their petrogenesis. Earth and Planetary Science Letters 38, 129–176.

Gorring, M.L., Kay, S.M., 2000. Carbonatite metasomatized peridotite xenoliths from southern Patagonia: implications for lithospheric processes and Neogene plateau magmatism. Contributions to Mineralogy and Petrology 140, 55–72.

Gregoire, M., McInnes, B.I.A., O'Reilly, S., 2001. Hydrous metasomatism of oceanic sub-arc mantle, Lihir, Papua New Guinea: Part 2. Trace element characteristics of slab-derived fluids. Lithos 59, 91–108.

Hickey, R.L., Frey, F., 1982. Geochemical characteristics of boninite series volcanics: implications for their source. Geochimica et Cosmochimica Acta 46, 2099–2115.

Hirose, K., Kushiro, I., 1993. Partial melting of dry peridotites at high pressures; determination of compositions of melts segregated from peridotite using aggregates of diamond. Earth and Planetary Science Letters 114 (4), 477–489.

Hole, M.J., LeMasurier, W.E., 1994. Tectonic controls on the geochemical composition of Cenozoic, mafic alkaline volcanic rocks from West Antarctica. Contributions to Mineralogy and Petrology 117 (2), 187–202.

Ionov, D., Hofmann, A.W., Shimizu, N., 1994. Metasomatism-induced Melting in Mantle Xenoliths from Mongolia. Journal of Petrology 35 (3), 753–785.

Ionov, D.A., O'Reilly, S., Genshaft, Y.S., Kopylova, M.G., 1996. Carbonate-bearing mantle peridotite xenoliths from Spitsbergen; phase relationships, mineral compositions and trace-element residence. Contributions to Mineralogy and Petrology 125 (4), 375–392.

Ionov, D.A., Gregoire, M., Prikhod'ko, V.S., 1999. Feldspar-Ti-oxide metasomatism in off-cratonic continental and oceanic upper mantle. Earth and Planetary Science Letters 165 (1), 37–44.

Jovanović, M., Downes, H., Vaselli, O., Cvetković, V., Prelević, D., Pecskay, Z., 2001. Paleogene mafic alkaline volcanic rocks of East Serbia. Acta Vulcanologica 13 (1–2), 159–173.

Karamata, S., Đorđević, P., 1980. Origin of the Upper Cretaceous and Tertiary magmas in the Eastern part of Yugoslavia. Bulletin Académie des Serbe des Sciences et des Arts, Classe des Sciences Mathématiques et naturelles, Sciences Naturelles, vol. LXXII (20), pp. 99–108.

Karamata, S., Knežević, V., Pécskay, Z., Đorđević, M., 1997. Magmatism and metallogeny of the Ridanj-Krepoljin belt (eastern Serbia) and their correlation with northern and eastern analogues. Mineralium Deposita 32, 452–458.

Karamata, S., Dimitrijević, N.M., Dimitrijević, D.M., 1999. Oceanic realms in the central part of the Balkan Peninsula during the Mesozoic. Slovak Geological Magazine 5 (3), 173–177.

Kelemen, P.B., Shimizu, N., Nobumichi, S., Vincent, J.M., 1995. Extraction of mid-ocean-ridge basalt from the upwelling mantle by focused flow of melt in dunite channels. Nature 375 (6534), 747–753.

Kilian, R., Franzen, C., Koch, M., Stern, B., Altherr, C.R., 1999. Metasomatism of the mantle wedge below the southern Andes. International Symposium on Andean Geodynamics, Okt. 1999 in Göttingen, Abstract Volume.

Kinzler, R.J., Grove, T.L., 1992. Primary magmas of mid-ocean ridge basalts; 1, experiments and methods. Journal of Geophysical Research, B, Solid Earth and Planets 97 (5), 6885–6906.

Kushiro, I., 1969. The system forsterite-diopside-silica with and without water at high pressures. The Schairer Volume, vol. 267-A. Kline Geology Laboratory Yale University, New Haven, CT, United States, pp. 269–294.

Laurent, R., Kacira, N., 1987. Chromite deposits in the Appalachian ophiolites. In: Stowe, W.C. (Ed.), Evolution of Chromium Ore Fields. Van Nostrand Reinhold, New York, N.Y., pp. 169–189.

Laurora, A., Mazzucchelli, M., Rivalenti, G., Vannucci, R., Zanetti, A., Barbieri, M.A., Cingolani, C.A., 2001. Metasomatism and melting in carbonated peridotite xenoliths from the mantle wedge: the Gobernador Gregores Case (Southern Patagonia). Journal of Petrology 42 (1), 69–87.

Macera, P., Gasperini, D., Piromallo, C., Blichert-Toft, J., Bosch, D., Del Moro, A., Martin, S., 2003. Geodynamic implications of deep mantle upwelling in the source of Tertiary volcanics from the Veneto region (South-Eastern Alps). Journal of Geodynamics 36, 563–590.

Maughan, D.T., Keith, J.D., Christiansen, E.H., Pulsipher, T.H., Keiko, E., Noreen, J., 2002. Contributions from mafic alkaline magmas to the Bingham porphyry Cu–Au–Mo deposit, Utah, USA. Mineralium Deposita 37 (1), 14–37.

Maury, R.C., Defant, M.J., Joron, J.L., 1992. Metasomatism of the sub-arc mantle inferred from trace elements in Philippine xenoliths. Nature 360 (6405), 661–663.

McDonough, W.F., Sun, S.-S., 1995. The composition of the Earth. Chemical Geology 120, 223–253.

McInnes, B.I.A., Cameron Eion, M., 1994. Carbonated, alkaline hybridizing melts from a sub-arc environment: Mantle wedge samples from the Tabar-Lihir-Tanga-Feni arc, Papua New Guinea. Earth and Planetary Science Letters 122, 125–141.

McInnes, B.I.A., Gregoire, M., Binns, R.A., Herzig, P.M., Hannington, M.D., 2001. Hydrous metasomatism of oceanic sub-arc mantle, Lihir, Papua New Guinea; petrology and geochemistry of fluid-metasomatised mantle wedge xenoliths. Earth and Planetary Science Letters 188 (1–2), 169–183.

Menzies, M., 1983. Mantle ultramafic xenoliths in alkaline magmas: evidence for mantle heterogeneity modified by magmatic activity. In: Hawkesworth, C.J., Norry, M.J. (Eds.), Continental Basalts and Mantle Xenoliths. Shiva Publications, pp. 92–110.

Morse, S.A., 1980. Kiglapait mineralogy II; Fe–Ti oxide minerals and the activities of oxygen and silica. Journal of Petrology 21 (4), 685–719.

Neumann, E.-R., Wulff-Pedersen, E., 1997. The origin of highly silicic glass in mantle xenoliths from the Canary Islands. Journal of Petrology 38 (11), 1513–1539.

Nicolas, A., Lucazeau, F., Bayer, R., 1987. Peridotite xenoliths in Massif Central basalts: textural and geophysical evidence for asthenospheric diapirism. In: Nixon, P.H. (Ed.), Mantle Xenoliths. Wiley, Chichester, pp. 563–574.

Pearce, N.J.G., Perkins, W.T., Westgate, J.A., Gorton, M.P., Jackson, S.E., Neal, C.R., Chenery, S.P., 1997. A compilation of new and published major and trace element data for the NIST SRM 610 and NIST SRM 612 glass reference materials. Geostandards Newsletter 21, 115–144.

Prelević, D., Foley, S.F., Romer, R.L., Cvetković, V., Downes, H., 2005. Tertiary ultrapotassic volcanism in Serbia: constraints on petrogenesis and mantle source characteristics. Journal of Petrology 46 (7), 1443–1487.

Santos, J.F., Schaerer, U., Gil Ibarguchi, J.I., Girardeau, J., 2002. Genesis of pyroxenite-rich peridotite at Cabo Ortegal (NW Spain); geochemical and Pb–Sr–Nd isotope data. Journal of Petrology 43 (1), 17–43.

Schmidt, G., Palme, H., Kratz, K.L., Kurat, G., 2000. Are highly siderophile elements (PGE, Re and Au) fractionated in the upper mantle of the earth? New results on peridotites from Zabargad. Chemical Geology 163 (1–4), 167–188.

Smith, D., Riter, J.C.A., 1997. Genesis and evolution of low-Al orthopyroxene in spinel peridotite xenoliths, Grand Canyon Field, Arizona. Contributions to Mineralogy and Petrology 127, 391–404.

Smith, D., Riter, J.C.A., Mertzman, S.A., 1999. Water–rock interactions, orthopyroxene growth, and Si-enrichment in the mantle: evidence in xenoliths from the Colorado Plateau, southwestern United States. Earth and Planetary Science Letters 165, 45–54.

Streckeisen, A., 1973. Plutonic Rocks. Classification and nomenclature recommended by the IUGS Subcommission on the Systematics of Igneous Rocks. Geotimes 18/10, 26–30.

Szabo, Cs., Bodnar, R.J., Sobolev, A.V., 1996. Metasomatism associated with subduction-related, volatile-rich silicate melt in the upper mantle beneath the Nograd-Gomor volcanic field, northern Hungary/ southern Slovakia; evidence from silicate melt inclusions, Fluid inclusions. Schweizerbart'sche Verlagsbuchhandlung 8, 881–899.

Varfalvy, V., Hebert, R., Bedard, J.H., 1996. Interactions between melt and upper-mantle peridotites in the North Arm Mountain massif, Bay of Islands ophiolite, Newfoundland, Canada: Implications for the genesis of boninitic and related magmas. Chemical Geology 129, 71–90.

Vlad, S.N., 1997. Calcic skarns and transversal zoning in the Banat Mountains, Romania; indicators of an Andean-type setting. Mineralia Deposita 32 (5), 446–451.

Wang, K.-L., Chung, S.-L., Chen, Ch.-H., 2002. Geochemical constraints on the petrogenesis of high-Mg basaltic andesites from the Northern Taiwan Volcanic Zone. Chemical Geology 182, 513–528.

Wendlandt, R.F., Eggler, D.H., 1980. The origins of potassic magmas: 2. Stability of phlogopite in natural spinel lherzolite and in the system KAlSiO4–MgO–SiO2–H2O–CO2 at high pressures and high temperatures. American Journal of Science 280, 421–458.

Witt-Eickschen, G., Klemd, R., Seck, H.A., 2003. Density contrast of fluid inclusions associated with melt (glass) from two distinct suites of mantle peridotites from the West Eifel, Germany: implications for melt origin. European Journal of Mineralogy 15, 95–102.

Xu, X., O'Reilly, S.Y., Griffin, W.L., Zhou, X., 2000. Genesis of young lithospheric mantle in southeastern China: an LAM-ICPMS trace element study. Journal of Petrology 41 (1), 111–148.

Xu, X., O'Reilly, S.Y., Griffin, W.L., Zhou, X., 1996. A xenolith-423-437. derived geotherm and the crust/mantle boundary at Qilin, southeast China. Lithos 38, 41–62.

Xu, X., O'Reilly, S.Y., Griffin, W.L., Zhou, X., 2003. Enrichment of upper mantle peridotite: petrological, trace element and isotopic evidence in xenoliths from SE China. Chemical Geology 198, 163–188.

Yaxley, G.M., Kamenetsky, V., Green, D.H., Falloon, T.J., 1997. Glasses in mantle xenoliths from western Victoria, Australia, and their relevance to mantle processes. Earth and Planetary Science Letters 148, 433–466.

Zanetti, A., Mazzucchelli, M., Rivalenti, G., Vannucci, R., 1999. The Finero phlogopite–peridotite massif; an example of subduction-related metasomatism. Contributions to Mineralogy and Petrology 134 (2–3), 107–122.